Intermediately Methylated Regions in Normal Cells Are Epimutation Hotspots in Cancer

Mohamed Mahgoub[1], Haley Abel[1], Nidhi Davarapalli[1], Heidi Struthers[1], Emilee Kotnik[1], Brittany Johnson[1], Christopher Markovic[2], Catrina Fronick[2], Robert Fulton[2], Michael P. Meers[3], and David H. Spencer*[1,2,4]

[1]Department of Medicine, Division of Oncology, Washington University School of Medicine; St. Louis, MO USA

[2]McDonnell Genome Institute, Washington University School of Medicine; St. Louis, MO USA

[3]Department of Genetics, Washington University School of Medicine; St. Louis, MO USA

[4]Department of Pathology and Immunology, Washington University School of Medicine; St. Louis, MO USA

* Corresponding author: dspencer@wustl.edu

Abstract

DNA methylation is altered in all cancers, but the mechanisms responsible for these changes are not well understood. Using data from 100 primary samples, we show that regions with intermediate methylation in normal hematopoietic cells are hotspots for stable, clonal epimutations in acute myeloid leukemia. Analysis of hematopoietic stem cell clones demonstrated that intermediate methylation at epimutation hotspots reflects random allele-specific methylation and expression at the single cell level, representing a previously unrecognized form of somatically acquired imprinting. We identified somatically imprinted regions in other tissues and show they are epimutation hotspots in other cancer types. This demonstrates that random allele-specific methylation is both a general property of normal cells, and a vulnerability that renders them susceptible to cooperating events and clonal selection during cancer.

Main text:

Cancer is caused by heritable somatic events that endow neoplastic cells with a selective advantage. While the most extensively studied somatic events in cancer are genetic mutations, cytosine methylation of DNA is also heritable through cell divisions and exhibits tissue-specific changes in malignant vs. normal cells. These include genome-wide methylation patterns present in most cancer types(*1–3*) and signatures that reflect a tumor's cell of origin, subtype and the effects of somatic mutations(*4–9*). Genome-wide studies have shown that abnormally methylated CpGs in cancer frequently cluster to form differentially methylated regions (DMRs)(*4*, *5*). However, the factors that determine why certain regions acquire these changes are poorly understood. This has made it difficult to define the mechanisms responsible for cancer-associated methylation changes and distinguish early events that could initiate cancer from alterations that are consequences of it(*4*, *10*).

Epimutations are spontaneous, heritable epigenetic abnormalities that can affect gene activity and cause human disease, including cancer(*11*, *12*). The best-characterized epimutations are inherited events that cause the imprinting disorders Beckwith-Wiedemann, Angelman, and Prader-Willi syndromes(*13*, *14*), or predispose patients to cancer via silencing of tumor suppressors(*15*, *16*). Epimutations can also be somatically acquired, most notably in cancer. These can also silence tumor suppressors, producing a second epigenetic 'hit' in tumors with a co-occurring somatic mutation(*17–19*). Although the mechanisms and timing of somatic epimutations are not well understood, there is evidence they may pre-exist in normal tissues(*20–24*) and could therefore be selected for during cancer development.

Although methylation in cancer has been extensively studied, most analysis has focused on changes associated with clinical or molecular features(*4*, *6*, *25–29*). Such approaches may be

52 less sensitive to detecting spontaneous epimutations, which could be independent of these
53 variables. Here, we used an unbiased analysis to identify somatically acquired DNA methylation
54 epimutations in acute myeloid leukemia (AML). Surprisingly, these events frequently occurred in
55 regions with intermediate methylation in normal hematopoietic cells, which harbor blocks of CpGs
56 that exhibit random allele-specific methylation in single cells. We demonstrate that methylation at
57 these blocks affects chromatin and gene expression, and that "somatically imprinted" regions are
58 epimutation hotspots in AML and other cancers.
59

60 **Intermediately methylated regions in normal hematopoietic cells are hotspots for altered**
61 **methylation in AML**

62 To identify DNA methylation changes in AML that could be somatically acquired
63 epimutations, we compared whole-genome bisulfite sequencing (WGBS) data from 100 primary
64 AML samples to WGBS from 16 purified hematopoietic cell populations from 7 healthy donors(*4*)
65 (Figure 1A, S1A). Pairwise comparisons were performed between each AML sample to pooled
66 data from stem/progenitor and mature myeloid cells (see Methods) to detect common and rare
67 events and account for maturation-related methylation changes in AML. Between 752 and 19,965
68 autosomal differentially methylated regions (DMRs) with a methylation difference >0.3 were
69 identified in each sample, for a total of 575,869 DMRs (Figure 1B, S1B). Merging of all DMRs
70 produced 76,752 unique regions, of which 33,181 (43.2%) were "private DMRs" in a single AML
71 sample, and 43,571 (56.8%) regions that overlapped DMRs identified in at least two samples
72 (Figure 1C). Applying a threshold of ≥25 AML samples resulted in 6,076 regions overlapping
73 recurrent DMRs that we defined as DMR "hotspots", which included regions near genes with
74 important roles in hematopoiesis and AML (e.g., *HOXA3*, Figure 1D).

We next investigated the normal epigenetic features at hotspots by annotating them with chromatin states(*30*) from hematopoietic stem/progenitor cells (HSPCs) (Figure S1C, see Methods). Hotspots were >10-fold enriched for bivalent chromatin and transcriptional initiation compared to private DMRs, which were evenly distributed across all states (Figure S1D-F). Interestingly, states with the highest enrichment for hotspots had intermediate methylation in normal HSPCs, an uncommon genomic feature that marks tissue-specific regulatory elements(*31*). Direct analysis showed that 48% of hotspots had intermediate methylation in normal HPSCs, and there was a 5-fold enrichment for intermediately methylated CpGs in hotspots compared to their genome-wide frequency (Figure 1E).

We next defined hematopoietic-specific intermediately methylated regions (IMRs) with methylation between 0.3 and 0.7 in normal hematopoietic cells and evaluated the hotspots overlapping these IMRs (i.e., "IMR hotspots") for features of somatic epimutations. Interestingly, methylation at IMR hotspots remained consistently intermediate throughout myeloid maturation and was present in promyelocytes, monocytes, and neutrophils (Figure 1F), and it was also stable between presentation and relapse in 6 AML patients (Figure S1H). Further, AML samples with DMRs at IMR hotspots showed consistent hyper- or hypomethylation at each hotspot, even in samples with mutations in *DNMT3A*, *IDH1*, *IDH2*, or *TET2* (Figures 1F, S1I) that cause directional methylation changes in AML(*4–6*). This implies that DMRs at IMR hotspots are not simply driven by these mutations. Finally, there was a modest but significant negative correlation between methylation at promoter-associated IMR hotspots and expression of nearby genes, supporting their functional role in gene regulation (Figure S1J). Together this demonstrates that intermediately methylated regions in normal cells are hotspots for methylation changes in AML that resemble somatically acquired epimutations.

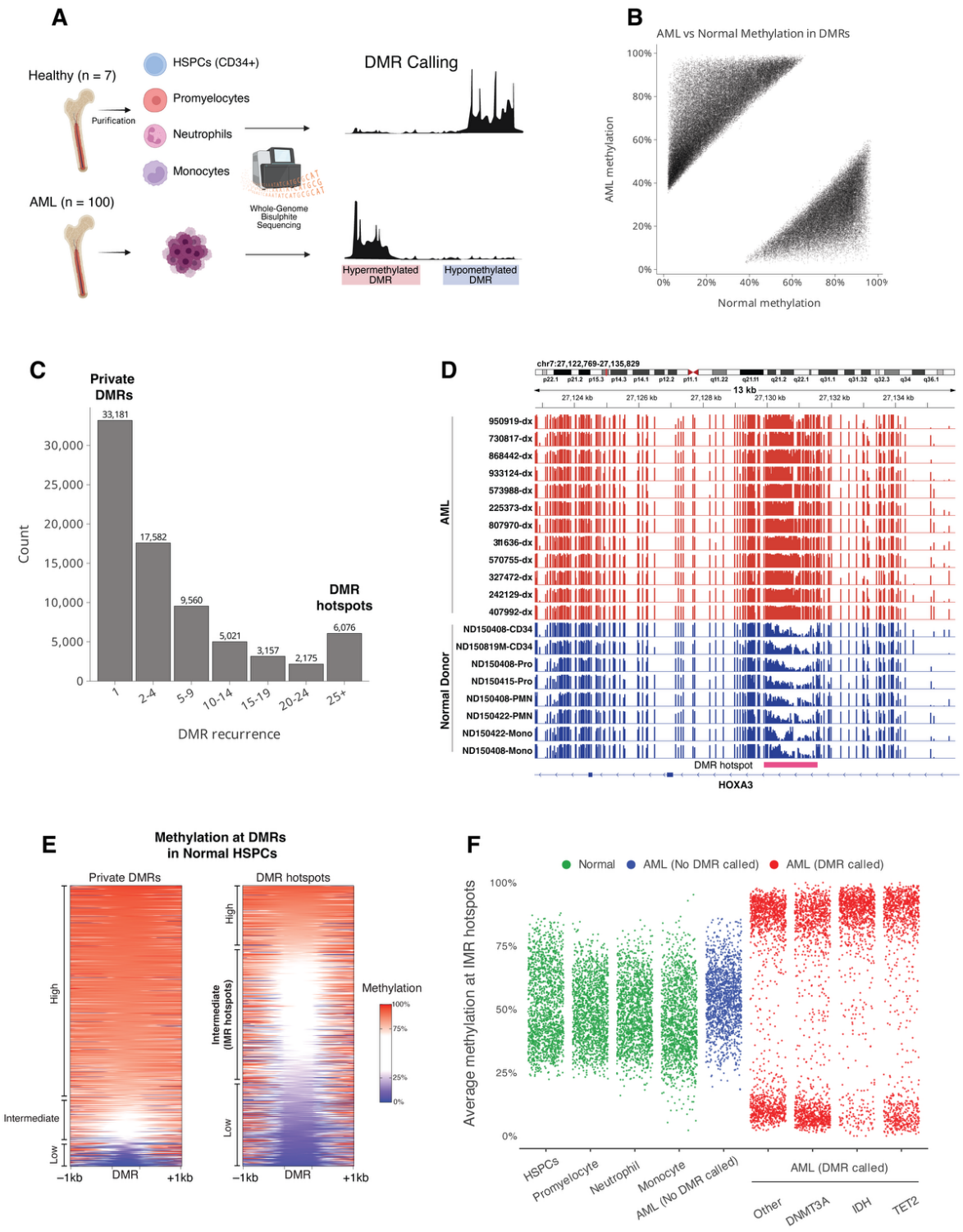
A
Healthy (n = 7)
Purification
HSPCs (CD34+)
Promyelocytes
Neutrophils
Monocytes
AML (n = 100)
Whole-Genome Bisulphite Sequencing
DMR Calling
Hypermethylated DMR
Hypomethylated DMR
B
AML vs Normal Methylation in DMRs
AML methylation
Normal methylation
C
Private DMRs
DMR hotspots
Count
DMR recurrence
33,181
17,582
9,560
5,021
3,157
2,175
6,076
D
chr7:27,122,769-27,135,829
13 kb
AML
Normal Donor
DMR hotspot
HOXA3
E
Methylation at DMRs in Normal HSPCs
Private DMRs
DMR hotspots
High
Intermediate
Low
Intermediate (IMR hotspots)
Methylation
DMR
F
Normal
AML (No DMR called)
AML (DMR called)
Average methylation at IMR hotspots
HSPCs
Promyelocyte
Neutrophil
Monocyte
AML (No DMR called)
AML (DMR called)
Other
DNMT3A
IDH
TET2

98

99 **Fig. 1**. **Recurrent differentially methylated regions in AML are enriched for intermediately**
100 **methylated regions in normal hematopoietic cells.**
101 (**A**) Analysis of differentially methylated regions (DMRs) in 100 primary AML samples. WGBS
102 data from each AML was compared to a pooled dataset of 16 hematopoietic cell populations
103 purified from bone marrow aspirates from 7 distinct healthy donors. (**B**) Scatter plot showing the
104 methylation level of each DMR identified in all AML samples versus mean methylation in normal
105 hematopoietic cells. (**C**) Recurrence of DMRs across AMLs after merging overlapping regions
106 from all samples. Private DMRs are regions with differential methylation in one AML sample,
107 while DMR hotspots are regions overlapping highly recurrent DMRs identified in at least 25 AML
108 samples. (**D**) DNA methylation at a DMR hotspot in the *HOXA3* locus from normal hematopoietic
109 cells and selected AML samples. (**E**) Heatmap showing methylation in normal hematopoietic
110 stem/progenitors (HSPCs) at regions overlapping private DMRs identified in only one AML
111 sample (left) and DMR hotspots (25+ samples) (right). DMRs are length-normalized and shown
112 with 1 kb of flanking sequence. (**F**) Methylation levels at intermediately methylated regions in
113 normal hematopoietic cells that are hotspots for differential methylation in AML samples (IMR
114 hotspots). Each point shows the mean methylation of IMR hotspot in the indicated normal
115 hematopoietic cell population (green), AMLs with no DMR called at the hotspot (blue), and AMLs
116 in which a DMR was called (red). AML samples with a DMR at the hotspots are grouped by the
117 presence of mutations in selected genes (minimum of 2 AML samples with the DMR hotspot per
118 mutation group).
119
120
121

122 **Intermediately methylated regions contain CpG blocks with allelic methylation in AML**

123 Intermediate methylation could be due to cellular heterogeneity, discordant methylation
124 across CpGs, or allele-specific methylation (Figure 2A). To distinguish between these possibilities,
125 we analyzed fragment-level methylation (*32*, *33*) at IMR hotspots in WGBS data from purified
126 normal hematopoietic cells. This showed that methylation at consecutive CpGs was highly
127 correlated at IMR hotspots compared to non-hotspot DMRs with intermediate methylation ($p<10^{-}$
128 ^{10}, Figure 2B, S2A). We next tested for allele-specific methylation (ASM) at IMR hotspots with
129 heterozygous SNPs in the normal and AML samples. Surprisingly, ASM was rare in normal
130 samples but more common in AML, especially in samples that retained intermediate methylation
131 (Figure 2C, S2B-C). To further explore this observation, we used Oxford Nanopore sequencing
132 (ONT) to obtain haplotype-resolved methylation from 10 primary AML samples and CD34+
133 HSPCs or immature (lineage marker-negative) bone marrow cells from four healthy donors (Figure
134 2D). We identified 1,264-4,497 autosomal regions of ASM per AML sample, after excluding
135 regions in imprinted genes, near structural variants, or with high SNP density; in comparison, ~300
136 ASM regions were identified in normal samples (Figure S2D). Interestingly, 30% of the IMR
137 hotspots overlapped an ASM region in the ONT data from AML samples, supporting our findings
138 from WGBS.

139 We next used the long-read ONT methylation data from all AML samples and normal
140 HSPCs to identify blocks of consecutive, highly correlated CpGs(*34*) that may be driving allelic
141 methylation at IMR hotspots. We also included published IMRs(*31*) and ASM regions from the
142 ONT data in this analysis, which we reasoned could share similar genomic features. This resulted
143 in 11,534 total methylation haplotype blocks, of which 1,575 had consistently intermediate
144 methylation in normal HSPCs (between 0.3 and 0.7), which we defined as "IMR blocks". These

145 blocks contained a mean of 12 CpGs, spanned 186 bp, and showed highly correlated—but
146 mosaic—patterns in HSPCs (Figure 2E). Analysis of haplotype-level methylation at all IMR
147 blocks from HSPCs showed that both haplotypes had intermediate methylation, matching the
148 aggregate methylation levels from ONT and WGBS (Figure 2F). In contrast, most IMR blocks in
149 AML samples either had ASM (Figure 2E and 2F: indicated in blue) or were fully
150 methylated/unmethylated on both alleles, reflecting an epimutation (Figure 2E and 2F: indicated
151 in yellow). These findings demonstrate the unique properties of IMR blocks, which have mosaic
152 haplotype-level methylation in normal cells that converts to ASM or fully
153 methylated/unmethylated epimutations in AML.
154

155 **Methylation at IMR blocks is associated with differential chromatin activity**

156 We next investigated whether methylation at IMR blocks is associated with differential
157 histone modifications using CUT&Tag and haplotype-level chromatin accessibility via Fiber-
158 seq(*35*). IMR blocks in HSPCs possessed both H3K27 and H3K4 trimethylation, consistent with
159 the bivalent chromatin states at hotspots from the HSPC-defined chromHMM model (Figure S2E).
160 In AML samples, both modifications were negatively correlated with methylation at IMR blocks,
161 with ASM blocks having intermediate signal consistent with allelic histone modification
162 differences (Figure 2G, S2F). Likewise, a negative correlation between methylation and
163 accessibility at IMR blocks was observed via Fiber-seq in two AML samples (Figure 2H). This
164 was also apparent at the haplotype level, with unmethylated haplotypes having higher accessibility
165 in aggregate and at individual regions (Figure 2I, 2J). Overall, these findings are consistent with
166 previous analysis of histone modifications at IMRs(*31*) and support a functional relationship where

167 unmethylated alleles at IMR blocks have greater accessibility and increased histone methylation

168 compared to methylated blocks.

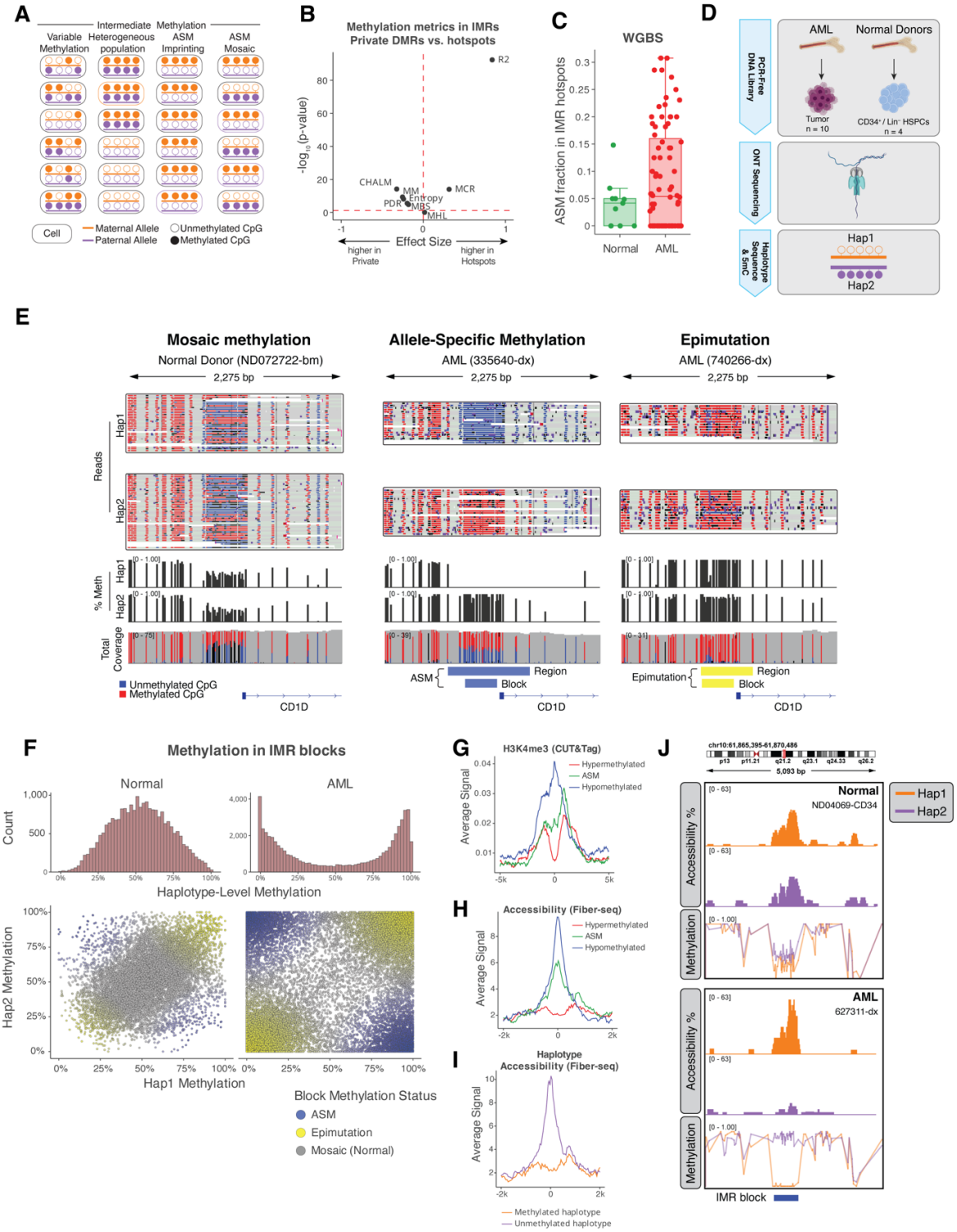

169

170 **Fig. 2. Intermediately methylated regions in normal hematopoietic cells display allelic**
171 **methylation patterns in AML**.
172 **(A)** Models of possible fragment-level methylation patterns at intermediately methylated regions
173 (IMRs). **(B)** Comparison of WGBS fragment-level methylation metrics at IMRs overlapping DMR
174 hotspots vs. non-hotspot DMRs in normal hematopoietic cells. Each point represents a different
175 metric, with the x-axis indicating the effect size (standardized difference in means between
176 hotspots and non-hotspots) and the y-axis indicating statistical significance as $-\log_{10}$(p-value) from
177 a t-test comparing the two groups. Metrics include PDR (Proportion of Discordant Reads), Entropy
178 (Shannon entropy), CHALM (Cell Heterogeneity-Adjusted cLoNal Methylation), R^2 (linkage
179 disequilibrium R squared), MHL (Methylation Haplotype Load), MCR (Methylation Concordance
180 Ratio), and MBS (Methylation Block Score). **(C)** Fraction of IMR hotspots exhibiting allele-
181 specific methylation (ASM) per sample from WGBS in normal hematopoietic cells and AML
182 samples, calculated among all IMR hotspots with a heterozygous SNP and sufficient coverage.
183 Only samples with at least 5 informative IMR hotspots are included. **(D)** ONT sequencing and
184 haplotype-resolved methylation analysis of normal HSPCs (N=4) and AML samples (N=10). **(E)**
185 Example of haplotype-resolved methylation in an IMR hotspot (at the promoter of *CD1D*),
186 showing mosaic methylation in normal hematopoietic cells, allele-specific methylation (ASM) in
187 AML sample 335640, and full methylation (epimutation) in AML sample 740266. Tracks show
188 the DMR region identified in each AML sample vs. normal cells using DSS R package and the
189 "IMR block" defined by correlation of fragment-level CpG methylation using ONT data(*34*). **(F)**
190 ONT haplotype-level methylation at IMR blocks in all normal HSPCs (N=4) and AML samples
191 (N=10). Top panels show the distribution haplotype-level methylation at IMR blocks. Bottom
192 panels show the average methylation of haplotype 1 versus haplotype 2 for each IMR block. **(G**

193 **and H)** Aggregated H3K4me3 CUT&Tag signal (G) and chromatin accessibility (Fiber-seq) (H)
194 at IMR blocks in AML samples, with blocks grouped by methylation status (hypomethylated,
195 intermediately methylated, or hypermethylated). **(I)** Chromatin accessibility (Fiber-seq) at IMR
196 blocks with intermediate methylation (green in panel H) and exhibiting ASM in AML samples,
197 comparing accessibility between the methylated and unmethylated haplotypes. **(J)** Example of
198 haplotype-resolved methylation and chromatin accessibility at an IMR block in an intergenic
199 region on chromosome 10 (chr10:61,866,122-61,869,606).
200

201 **Allelic methylation at IMR blocks is stable over time and marks clonal hematopoiesis**

202 To determine the stability of allelic methylation at IMR blocks, we used ONT sequencing
203 to analyze paired presentation/relapse samples from 3 AML patients who relapsed after
204 chemotherapy with a related AML clone (Figure 3A, S3A). We compared IMR blocks with allelic
205 methylation (i.e., ASM or a methylated/unmethylated epimutation) between presentation and
206 relapse samples for each patient (using synchronized haplotype designations), which demonstrated
207 that >92.5% of the ASM blocks and >98.9% of the blocks with epimutations were stable at relapse.
208 We next tested whether allelic methylation at IMR blocks is specific to leukemic cells by analyzing
209 remission samples from two of the AML patients. Whole-genome sequencing(*36*) confirmed a
210 molecular remission in patient 895870, while patient 627311 had a persistent *DNMT3A* mutation
211 and several noncoding exome variants, indicating the presence of clonal hematopoiesis (Figure
212 S3B). Patient 895870 had allelic methylation at IMR blocks at presentation that nearly completely
213 normalized in the remission sample before returning at relapse (Figure 3C). Interestingly, allelic
214 methylation only partially normalized in the remission sample from patient 627311 that had clonal

215 hematopoiesis, which instead retained a pattern closer to the presentation and relapse samples
216 (Figure 3D).

217 To further examine the relationship between allelic methylation at IMR blocks and clonal
218 hematopoiesis, we used ONT sequencing to measure methylation in additional remission samples
219 from 4 patients who had either complete clearance of somatic mutations or multiple persistent
220 mutations by exome sequencing, indicating clonal hematopoiesis(*36*) (Figure 3E, S3C).
221 Quantification of IMR blocks with allelic methylation showed that patients with clonal
222 hematopoiesis had a significantly higher fraction of allelic blocks compared to samples with
223 complete mutation clearance (41% vs. 22%; p=0.034, Student's *t*), supporting an association of
224 ASM and epimutations with clonal hematopoiesis.

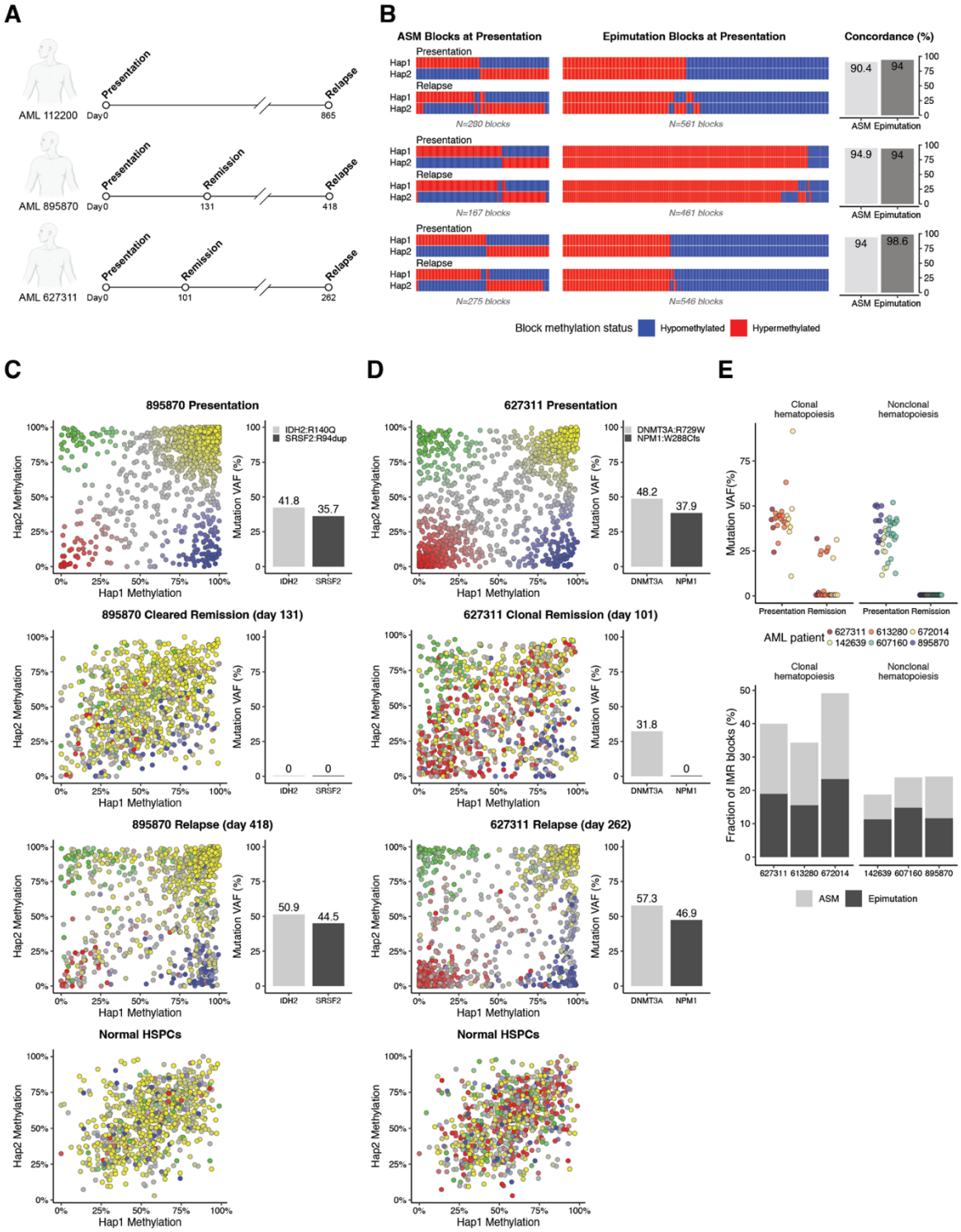
A
AML 112200
Presentation
Relapse
Day0
865
AML 895870
Presentation
Remission
Relapse
Day0
131
418
AML 627311
Presentation
Remission
Relapse
Day0
101
262
B
ASM Blocks at Presentation
Epimutation Blocks at Presentation
Concordance (%)
Presentation
Relapse
Hap1
Hap2
N=280 blocks
N=561 blocks
90.4
94
N=167 blocks
N=461 blocks
94.9
94
N=275 blocks
N=546 blocks
94
98.6
ASM Epimutation
Block methylation status
Hypomethylated
Hypermethylated
C
895870 Presentation
IDH2:R140Q
SRSF2:R94dup
41.8
35.7
895870 Cleared Remission (day 131)
0
0
895870 Relapse (day 418)
50.9
44.5
Normal HSPCs
Hap2 Methylation
Hap1 Methylation
Mutation VAF (%)
IDH2
SRSF2
D
627311 Presentation
DNMT3A:R729W
NPM1:W288Cfs
48.2
37.9
627311 Clonal Remission (day 101)
31.8
0
627311 Relapse (day 262)
57.3
46.9
Normal HSPCs
DNMT3A
NPM1
E
Clonal hematopoiesis
Nonclonal hematopoiesis
Mutation VAF(%)
Presentation
Remission
AML patient
627311
613280
672014
142639
607160
895870
Fraction of IMR blocks (%)
ASM
Epimutation

225

226

227 **Fig. 3. IMR blocks are stable, clonal events in hematopoietic cell populations. (A)**
228 Longitudinal analysis of methylation at IMR blocks in 3 AML patients (112200, 895870, and
229 627311) who achieved a complete morphologic remission with standard "7+3" induction
230 chemotherapy. ONT sequencing was performed on the samples at the timepoints indicated by the
231 open circles. **(B)** Heatmap representation of haplotype-level methylation from ONT sequencing of
232 paired presentation/relapse sample pairs. IMR blocks were classified as either having ASM (left)
233 or a fully methylated/unmethylated epimutation (right) via Fisher's exact test on methylation read
234 counts either between haplotypes (for ASM) or compared to normal HSPCs (for epimutations).
235 Methylated and unmethylated IMR blocks are shown in red and blue, respectively. Only IMR
236 blocks with statistically significant classifications at both presentation and relapse are shown. The
237 percent of concordant ASM and epimutation blocks between presentation and relapse is shown on
238 the right. **(C)** Haplotype-level methylation at IMR blocks from AML patient 895870 at
239 presentation, complete morphologic and molecular remission (i.e., blasts <1% and no leukemia-
240 associated mutations detected), and relapse. Points show the methylation of IMR blocks in
241 haplotype 2 vs. haplotype 1 and are colored by their methylation status in the presentation sample.
242 Bar plots show the variant allele fraction (VAF) of selected recurrent mutations in each sample.
243 Bottom panel shows haplotype-level methylation at the same IMR blocks from a representative
244 CD34+ HSPC sample and are colored based on the methylation status of the block in the
245 presentation AML sample. **(D)** Haplotype-level methylation in AML patient 627311 at
246 presentation, complete morphologic remission (bone marrow blasts <1%), but with a persistent
247 *DNMT3A*, and relapse. Scatter plots are shown as in (C). Bar plots show mutation VAFs in each
248 sample and indicate the presence of a *DNMT3A*^{R729W} variant in the remission sample, consistent
249 with persistent clonal hematopoiesis. **(E)** Correlation between clonal hematopoiesis in AML

250 remission and the presence of ASM and epimutations at IMR blocks from ONT sequencing. Top
251 panels show mutation VAFs at presentation and complete remission for 6 patients, 3 with clonal
252 hematopoiesis in remission (left) and 3 with nonclonal hematopoiesis. Bottom panel shows the
253 fraction of all IMR blocks (N=1,575) that met criteria for being ASM or fully
254 methylated/unmethylated epimutations compared to normal HSPCs in each sample using a
255 Fisher's exact test on haplotype-level methylation read counts. All remission samples were bone
256 marrow aspirates with normal trilineage hematopoiesis and <1% blasts. See reference (*36*) .
257

258 **Random allele-specific methylation at IMR blocks is somatically acquired in normal**
259 **hematopoietic stem cells**

260 We reasoned that intermediate methylation at IMR blocks could reflect random ASM that
261 is developmentally established in HSPCs at the single cell level and thus can be observed in clonal
262 AML samples and clonal hematopoiesis but not in bulk cell populations. To test this, we examined
263 IMR block methylation in ONT data from human embryonic stem cells. This showed that most
264 blocks were fully methylated or unmethylated on both haplotypes (Figure S4A), implying that
265 intermediate methylation emerges during hematopoietic development. IMR blocks also reverted
266 to being fully methylated or unmethylated in induced pluripotent stem cells derived from CD34+
267 HSPCs(*37*) (Figure S4B), indicating these states are intrinsic to pluripotent stem cell identity.

268 To determine whether mosaic methylation at IMR blocks reflects random ASM, we sorted
269 CD34+/CD38-/CD45RA- HSCs from primary cord blood and expanded bulk HSCs and 11 single-
270 cell HSC clones for analysis via ONT sequencing (Figure 4A). This showed that methylation at
271 most IMR blocks with intermediate methylation in bulk HSCs (684 of 1,575 blocks) did not have
272 mosaic methylation at the haplotype level in single HSC clones: 69% of blocks had ASM in at

273 least one clone and most clones had either ASM or were fully methylated/unmethylated on both
274 haplotypes (Figure 4B). Further, 83% of IMR blocks with ASM in ≥4 clones (N=164) showed
275 'switching' of the methylated haplotype, implying stochastic selection of the methylated state
276 (Figure 4C, 4D). In comparison, haplotype-level methylation was consistent in 98% of regions
277 with ASM in bulk HSCs (Figure 4C), indicating that the random methylation is unlikely to be due
278 to technical or biologic variability. IMR blocks with hyper or hypomethylated epimutations in the
279 HSC clones were also random, but to a lesser extent, with 44% of blocks switching between full
280 hyper and hypomethylated epimutations (Figure S4C, S4D). Most of the epimutation blocks had
281 increased methylation, an effect previously observed in cells forced to rapidly divide in culture(*4*,
282 *38*).

283 We next tested whether random ASM could be linked to allele-specific expression (ASE)
284 by performing bulk RNAseq on 6 HSC clones. Although we were limited to examining only genes
285 with coding SNPs near IMR blocks, we identified a block in an internal promoter of *SCHIP1* with
286 intermediate methylation in bulk HSCs that was either fully methylated/unmethylated or had ASM
287 in all 6 clones (Figure 4E). Haplotype-level expression of *SCHIP1* isoforms using this promoter
288 was variable and correlated with IMR block haplotype methylation. Similar effects were seen for
289 *GATA2*, a critical gene in hematopoietic development previously shown to have ASE in AML(*17*,
290 *22*); several ASM regions were present at the *GATA2* locus in our data, but these did not meet all
291 IMR block criteria. However, *GATA2* had striking monoallelic expression in two clones, and the
292 expression level correlated with haplotype-level methylation in a block-like region (Figure S4E),
293 indicating that both ASM and ASE at *GATA2* are pre-existing states in normal HSCs. Together
294 these observations imply that IMR blocks like those at the *SCHIP1* and *GATA2* loci undergo a
295 form of somatically acquired "imprinting" during hematopoietic development.

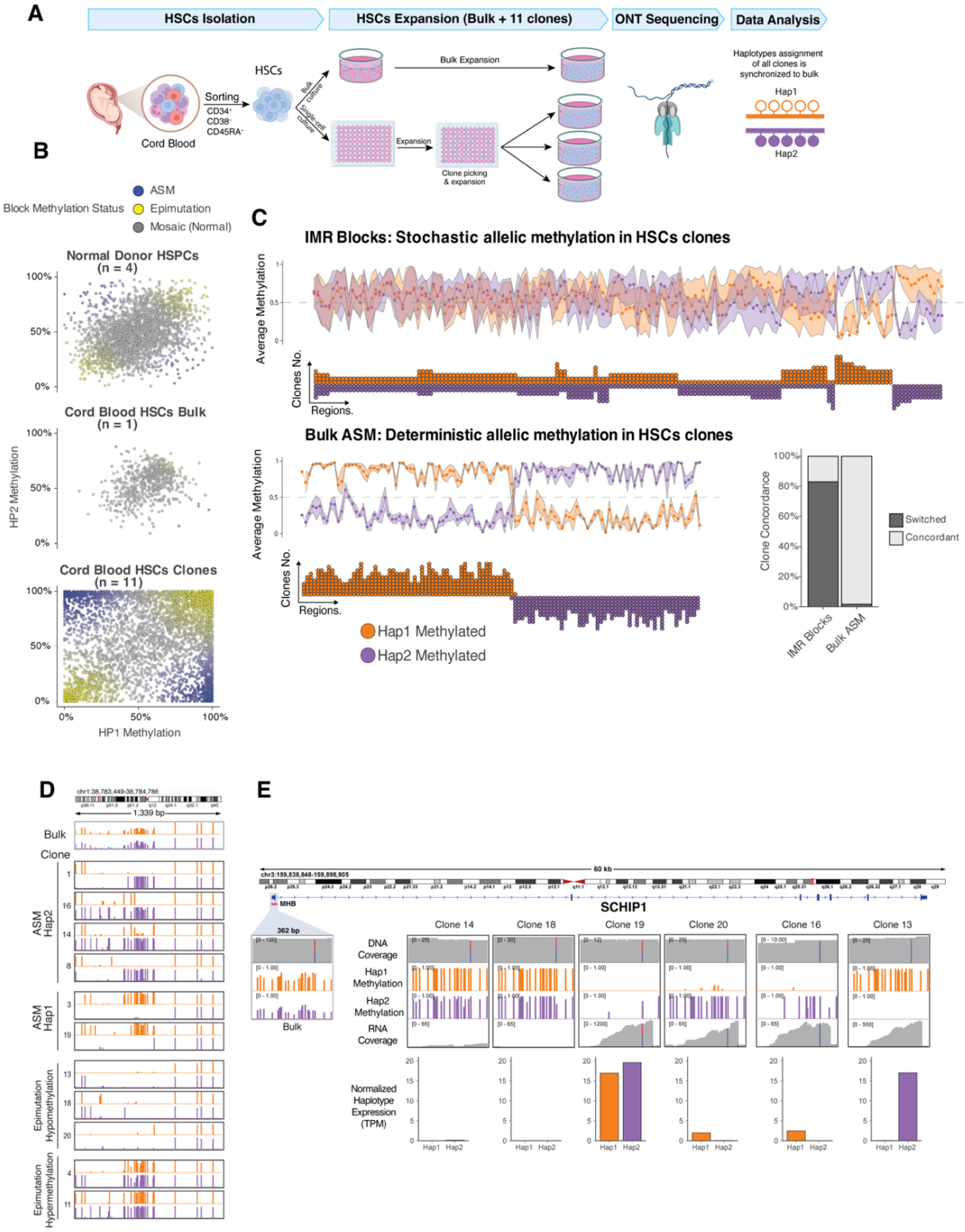
A
HSCs Isolation
HSCs Expansion (Bulk + 11 clones)
ONT Sequencing
Data Analysis
Cord Blood
Sorting
CD34+
CD38-
CD45RA-
HSCs
Bulk culture
Single-cell culture
Bulk Expansion
Expansion
Clone picking & expansion
Haplotypes assignment of all clones is synchronized to bulk
Hap1
Hap2
B
Block Methylation Status
ASM
Epimutation
Mosaic (Normal)
Normal Donor HSPCs (n = 4)
Cord Blood HSCs Bulk (n = 1)
Cord Blood HSCs Clones (n = 11)
HP2 Methylation
HP1 Methylation
C
IMR Blocks: Stochastic allelic methylation in HSCs clones
Average Methylation
Clones No.
Regions.
Bulk ASM: Deterministic allelic methylation in HSCs clones
Hap1 Methylated
Hap2 Methylated
Clone Concordance
Switched
Concordant
IMR Blocks
Bulk ASM
D
1,339 bp
Bulk
Clone
ASM Hap2
ASM Hap1
Epimutation Hypomethylation
Epimutation Hypermethylation
E
60 kb
SCHIP1
MHB
362 bp
Bulk
Clone 14
Clone 18
Clone 19
Clone 20
Clone 16
Clone 13
DNA Coverage
Hap1 Methylation
Hap2 Methylation
RNA Coverage
Normalized Haplotype Expression (TPM)
Hap1
Hap2

296

297 **Fig. 4. Random allele-specific methylation at IMR blocks is established in single**
298 **hematopoietic stem cells and is associated with allele-specific gene expression.**
299 **(A)** HSC expansion and sequencing to analyze haplotype-level methylation in single-cell-derived
300 HSC clones. **(B)** Haplotype-level methylation at IMR blocks in normal donor HSPCs, bulk cord
301 blood HSCs, and single-cell-derived HSC clones. Each point corresponds to the average
302 methylation of one IMR block within a single clone. Only IMR blocks with intermediate
303 methylation (0.3–0.7) in the bulk HSCs were included. **(C)** Haplotype-level methylation patterns
304 in single-cell-derived HSC clones at IMR blocks exhibiting intermediate methylation in bulk HSCs
305 (top, labelled "IMR Blocks") and regions showing allele-specific methylation (ASM) in bulk
306 HSCs (bottom left, "Bulk ASM"). In both panels, line plots display the average methylation of
307 haplotype 1 (orange) and haplotype 2 (purple) across all clones for each region. The dot plots
308 below indicate the number of individual clones in which Haplotype 1 or Haplotype 2 was
309 methylated, which is indicated by the Y-axis and the dot color. The bar plot (bottom right)
310 quantifies the percentage of regions where the methylated allele is concordant across clones versus
311 switched (i.e., random) for both IMR blocks and bulk ASM regions. Only regions with ASM
312 observed in at least four clones were included in this analysis. **(D)** Example of an IMR block
313 exhibiting random methylation patterns in HSC clones. The tracks display haplotype-level
314 methylation at the block that shows intermediate methylation in bulk HSCs. Individual clones
315 demonstrate random allele-specific methylation (ASM) on either haplotype 1 (orange) or
316 haplotype 2 (purple), or an epimutation showing either fully hypomethylated or hypermethylated
317 states. **(E)** Allele-specific methylation is associated with allele-specific expression in HSC clones
318 at an IMR block located within an internal promoter of the *SCHIP1* gene. For several
319 representative clones, tracks display DNA coverage, haplotype 1 methylation (orange), haplotype

320 2 methylation (purple), and RNA coverage. The bar plots quantify normalized, haplotype-specific
321 expression in Transcripts Per Million (TPM). RNA Reads are assigned to haplotypes based on a
322 heterozygous SNP, which is indicated by the vertical blue/grey (haplotype 1) and red (haplotype
323 2) lines in the coverage tracks. While DNA coverage is consistently biallelic, the level of RNA
324 expression from each haplotype is inversely correlated with its methylation status, demonstrating
325 that higher methylation is linked to transcriptional repression.
326

327 **Intermediately methylated blocks in multiple normal tissues are epimutation hotspots in**
328 **cancer**

329 We were next interested in whether IMR blocks in other tissues displayed epigenetic
330 features like those in hematopoietic cells and were associated with abnormal methylation in
331 tumors. For this analysis, we used data from a recent study of methylation in normal tissues that
332 defined tissue-specific CpG blocks with bimodal methylation (i.e., IMR blocks) (*39*, *40*), as well
333 as separate studies of primary tumors using WGBS or ONT(*41–44*) (Figure 5A). Interestingly, the
334 published set of IMR blocks were enriched for bivalent chromatin and transcriptional start sites in
335 all tissues, similar to the blocks we identified in hematopoietic cells (Figure 5B, see also Figure
336 S1). Likewise, analysis of haplotype-level methylation from primary tumors showed that these
337 blocks lost intermediate methylation and frequently had ASM. Haplotype-level analysis showed
338 that 25-71% of IMR blocks with retained intermediate methylation had ASM across tumor types,
339 further indicating that ASM in these regions is a property of clonal cell populations (Figure 5C,
340 5D).

341 Finally, we sought to determine whether IMR blocks are hotspots for altered methylation
342 in solid tumors and could therefore represent epimutations. Indeed, methylation at tissue-specific

343 IMR blocks was frequently altered in both ONT and WGBS tumor data (Figure 5E, S5A). We then
344 quantified the frequency of altered methylation at IMR blocks by comparing block methylation in
345 each tumor sample to its respective normal tissue. For comparison, the same analysis was
346 performed using other genomic regions commonly associated with differential methylation in
347 cancer, including CpG islands, gene promoters and tissue-specific enhancers defined via chromatin
348 states(*30*). Surprisingly, the fraction of IMR blocks with differential methylation was the highest
349 among these regions, with a mean of 40% to 65% having statistically significant differential
350 methylation vs. normal tissue (Figure 5F, S5B). By comparison, 3.6% to 22% of the other regions
351 had differential methylation across tumor types. This demonstrates that tissue-specific CpG blocks
352 with intermediate methylation are "hotspots" for altered methylation in multiple tumor types.
353

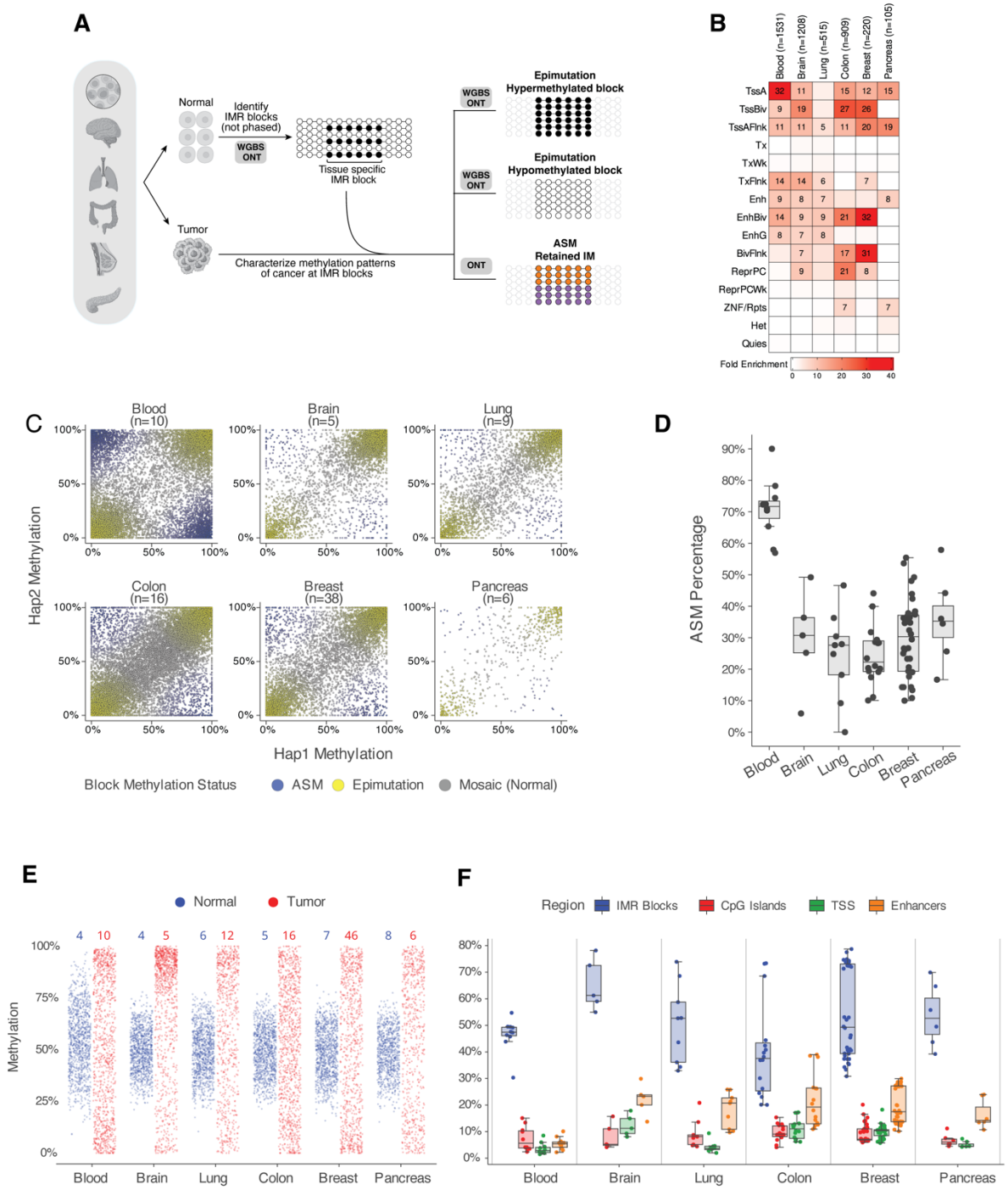

Fig. 5. Tissue-specific IMRs in normal cells are hotspots for epimutations in cancer.

(A) Identifying methylation changes at tissue-specific intermediately methylated regions (IMRs) in multiple cancers. IMRs for hematopoietic cells were identified using ONT data from this study,

359 while IMRs for other tissues were defined using a normal tissue WGBS atlas(*39*). For each tissue,
360 epimutations (hyper- or hypo-methylation) were identified by comparing tumor samples to their
361 normal counterparts. Allele-specific methylation (ASM) was called using haplotype-phased ONT
362 data. This analysis integrated data for AML generated in this study with published datasets for
363 other cancers, including ONT(*41*) and WGBS(*42*, *44*) data. For details, see the Methods section.
364 **(B)** Heatmap showing the fold enrichment of tissue-specific IMRs within tissue-specific chromatin
365 states. For each tissue (columns), the enrichment of its specific IMRs (n = number of blocks) was
366 calculated for each chromatin state (rows) relative to a genomic background. Values displayed
367 represent the fold enrichment for regions with an enrichment of ≥5. Chromatin state annotations
368 were obtained from the Roadmap Epigenomics Consortium(*45*) . **(C)** Comparison of Haplotype 1
369 versus Haplotype 2 methylation at tissue-specific IMRs in cancer samples using ONT data**. (D)**
370 Percentage of tissue-specific IMRs with retained intermediate methylation (0.3-0.7) that exhibit
371 allele-specific methylation (ASM) per sample in various cancer types, using phased ONT data.
372 Each point represents an individual tumor sample. The box plots summarize the distribution of
373 ASM percentages for each cancer type shown. **(E)** Distribution of average methylation levels at
374 tissue-specific IMRs in normal tissues (blue) and their corresponding primary tumors (red) from
375 ONT data. The numbers at the top of the plot indicate the number of samples included in each
376 group. Each point represents the average methylation of a single IMR block within a sample, with
377 data from multiple samples pooled for each tissue type. For visualization, 1,000 points were
378 randomly sampled for each group. Data for tumor samples and normal blood were derived from
379 ONT, while data for other normal tissues were from WGBS. **(F)** Percentage of various genomic
380 features exhibiting epimutations across different cancer types from ONT data for individual
381 primary tumor samples. Epimutations were defined as a significant difference in aggregate

382 methylation via a Fisher's exact test on methylation counts for each region between tumor and its
383 respective normal. Boxplots show the percentage of tissue-specific IMRs (IMR Blocks), CpG
384 islands, tissue-specific transcriptional start sites (TSS), and tissue-specific enhancers that have
385 significant count-based differential methylation in each tumor sample compared to its
386 corresponding normal tissue.
387
388 **Discussion**
389 The factors that predispose certain regions to DNA methylation changes in cancer are not
390 well understood. Here we showed that discrete blocks of CpGs with intermediate methylation in
391 normal cells are *a priori* hotspots for methylation changes in AML and multiple solid tumors. In
392 AML, methylation changes at intermediately methylated regions (IMRs) resemble epimutations:
393 they are stable, clonal events that are less dependent on mutation-driven phenotypes and can be
394 observed in non-leukemic cells. Further, intermediate methylation at these blocks in normal
395 hematopoietic cells is caused by random allele-specific methylation at the single cell level. The
396 highly tissue-specific and stable nature of methylation at these regions implies they normally
397 undergo a type of developmental "somatic imprinting", and epimutations in AML are due to the
398 absence of this allele-specific state. Further, these regions possess active and bivalent chromatin
399 features and occur near important tissue-specific genes, which suggests they are involved in gene
400 regulation and could be subject to selection during AML pathogenesis.
401 The concept of allele-specific somatic imprinting is consistent with previous epigenetic
402 studies in primary human tissues. In hematopoietic cells, clonal cell populations exhibit heritable,
403 random monoallelic gene expression(*21*, *22*), and separate studies have used methylation
404 signatures as clonal markers(*46*, *47*). The blocks of random allele-specific methylation described

405 here provide a direct link between these observations by identifying discrete loci where
406 methylation can both contribute to gene regulation and encode stable markers of clonal identity.
407 While it is possible that the mosaic methylation pattern of these regions means they are less
408 functionally relevant, their relationship to chromatin activity and expression suggests otherwise.
409 The striking consistency and stability of IMRs in HSCs also implies that establishing intermediate
410 methylation via somatic imprinting could be a defining feature of HSC identity; epimutations could
411 then be caused by a failure or spontaneous loss of imprinting. While the forces that make ASM
412 advantageous are unknown, it could enable precise gene dosage or simultaneous transcription of
413 two closely spaced genes from opposite alleles. Notably, the *GATA2*, *SCHIP1* and *HOXA* loci with
414 ASM all encode multiple overlapping transcripts and could be subject to such constraints.

415 One consequence of somatic imprinting is that it generates a substrate for selection during
416 cancer development. For example, genes with ASM and monoallelic expression would be
417 vulnerable to somatic mutations as a second hit(*17*, *18*). Likewise, the presence of epimutations is
418 a source of epigenetic heterogeneity that could confer an advantage to some cells. We found that
419 IMR blocks were differentially methylated more often than CpG islands, promoters, and enhancers
420 in multiple cancers, and in AML, individual IMR blocks tended to become either fully methylated
421 or unmethylated, hinting that certain epimutations may be under selection. The discrete nature of
422 these events means they may be more amenable to direct measurements and functional
423 characterization to understand how pre-existing epigenetic variability contributes to the somatic
424 processes that lead to cancer.
425

426 **Materials and Methods**
427
428 *Primary AML and normal hematopoietic cell samples*

429 Primary AML and normal hematopoietic cell samples used in this study were collected from
430 consented subjects using IRB-approved protocols (WashU HRPO#201011766, FHCC #985.03).
431 AML samples were either peripheral blood or bone marrow aspirate specimens obtained from
432 patients with active disease at presentation or relapse and were processed without fractionation,
433 purification, or enrichment via buffy coat preparation into cryopreserved cell suspensions or
434 directly used for DNA extraction (see Tables S1 and S4). Remission samples were unfractionated
435 whole bone marrow aspirates or peripheral blood samples obtained from patients in morphologic
436 complete remission at the timepoints indicated in Figure 3. Normal adult CD34+ HSPCs,
437 promyelocytes, neutrophils, and monocytes from healthy donor bone marrow aspirate samples as
438 described previously(*4*, *5*). Additional HSPC data were generated from two sources. First, we
439 used peripheral blood mobilized CD34+ HSPCs from 3 donors from the Fred Hutchinson Cancer
440 Center (FHCC) Cooperative Centers of Excellence in Hematology Cell Procurement &
441 Processing Core. Second, we enriched for lineage-negative cells from bone marrow aspirates
442 from two healthy adult donors via bead-based depletion of lineage-positive cells (Miltenyi cat#
443 130-092-211) on an autoMACS instrument (Miltenyi). Finally, commercially available purified
444 CD34+ HSPCs from cord blood samples (STEMCELL) were used for the clonal expansion
445 experiment.
446

447 *Cord blood HSC sorting and expansion*

448 Cryopreserved umbilical cord blood CD34+ cells (10^6 cells from a single donor purchased from
449 STEMCELL Technologies) were thawed in a ThawSTAR instrument (BioLife) and then cultured

450 overnight in 10 wells of a 96-well U-bottom plate in StemSpan media with CD34+ expansion
451 supplement, UM729 (STEMCELL) and 1% pen/strep antibiotic. After overnight culture, cells
452 were collected and stained with CD34-APC (BD Pharmingen, #555824), CD38-PE (BD
453 Pharmingen, #560981), CD45RA-FITC (BD Pharmingen, #561882) and Near-IR LIVE/DEAD
454 stain (Invitrogen) for FACS on a MoFlo instrument. Single CD34+/CD38-/CD45RA- cells were
455 sorted into two 96-well flat-bottom plates seeded with 25,000 cells/well of irradiated (2000 cGy)
456 AFT024 stroma (ATCC) and containing 100 uL of prepared StemSpan media. An additional
457 30,000 cells with the same immunophenotype were sorted into an additional well for expansion
458 of a bulk (nonclonal) cell population. On days 4 and 10 after sorting 50 uL of prepared StemSpan
459 media was added to all wells. The bulk HSCs were harvested in day 15 of culture and yielded
460 approximately 10^7 cells. Expanded single-cell clones were transferred to 24-well plates without
461 AFT024 stroma on days 21 and 23 of culture and then expanded in 0.5 mL of prepared
462 StemSpan media for an additional 4 days before harvesting for DNA and RNA extraction.
463
464 *Human embryonic stem cell and iPS cell culture*
465 Human WA0, WA09/H9 ESCs and BM9 iPSCs were cultured in mTESR media (STEMCELL)
466 and passaged using dispase before harvesting for DNA extraction.
467
468 *Whole-genome bisulfite sequencing data production*
469 WGBS data from 51 AML samples and 15 normal hematopoietic cell populations were
470 repurposed from prior studies(*4*, *5*). Additional datasets were generated as described
471 previously(*5*) using the Zymo Gold Bisulfite conversion (Zymo Research) and Accel DNA
472 methylation kit (IDT) kits to generate WGBS libraries. QC was performed on Agilent

473 Bioanalyzer or Tapestation instruments prior to sequencing on NovaSeq 6000 or X plus
474 instruments to generate 2x150 paired end reads to a target genome coverage of 10x. All WGBS
475 data were processed using the DRAGEN software suite (v4.2.4) to obtain genome-wide 5mC
476 read counts and methylation fractions.
477
478 *ONT sequence data production and processing*
479 All DNA for ONT sequencing was extracted using either the NEB Monarch or QIAmp DNA
480 mini kit. DNA was fragmented and size-selected to eliminate small (<5 kbp) fragments and then
481 prepared for sequencing via the LSK114 kit and sequenced using R10.4.1 flowcells on a
482 PromethION sequencer (Oxford Nanopore Technologies, Oxford, UK) with up to two
483 wash/reload cycles. For data obtained from expanded HSCs, adaptive sampling was performed
484 for all IMRs and ASM regions identified in AML samples. Data processing and analysis,
485 including basecalling, was performed via a Nextflow workflow (https://github.com/dhslab/nf-
486 core-wgsnano, commit 8fe4655) using dorado (v0.5.2+7969fab) for basecalling and read
487 mapping, and the PEPPER-Margin-Deepvariant pipeline for phased germline variant calling of
488 SNV and small indels (v0.8.0)(*54*). Structural variants were identified after data processing using
489 Sniffles(*55*). Haplotagging was performed using Whatshap (v2.2)(*56*), which used a common
490 phased VCF file for presentation/remission/relapse samples from AML patients and the bulk
491 HSC data for the HSC expansion experiment to synchronize the haplotype designations.
492 Mosdepth (v.0.3.3)(*57*) was used to calculate coverage. Combined and haplotype-specific 5mC
493 counts were generated with modkit (https://github.com/nanoporetech/modkit).
494
495 *Fiber-seq on normal HSPCs and primary AML samples*

496 Fiber-seq was performed on cryopreserved mobilized CD34+ HSPCs from two donors (obtained
497 from FHCC) and presentation/relapse sample pairs from two AML patients using the published
498 protocol(*41*) with slight modifications. Cells were thawed in a ThawSTAR instrument and $2x10^6$
499 cells were collected at 250xg for 5 minutes, washed once in 1mL cold PBS and resuspended in
500 120 uL CUT&TAG nuclear extraction buffer (20 mM HEPES-KOH, pH 7.9, 10 mM KCl, 0.1%
501 Triton X-100, 20% glycerol, and 0.5mM spermidine) and incubated for 10 minutes on ice.
502 Nuclei were then collected at 350xg for 5 minutes and resuspended in 60 uL Buffer A (15mM
503 Tris-HCl, 15 mM NaCl, 60 mM KCl, and 1 mM EDTA, pH 8.0) and transferred to a PCR tube
504 before adding 1.5 uL 32 mM s-adenosyl methionine (SAM) and 0.5 uL Hia5 enzyme (200U/uL,
505 a gift from A. Stergachis). Reactions were incubated at 25C in a thermocycler for 10 min and
506 then stopped with 6uL of 10% SDS (final concentration of 1%). The lysate was transferred to a
507 1.5mL tube with wide bore tips and stored at -80C prior to DNA extraction and sequencing.
508 DNA was extracted with a MagAttract DNA extraction kit, fragmented with a megaruptor and
509 size-selected on a HTpippen to 18-22kbp prior to SMRTbell library preparation. Libraries were
510 sequenced on a PacBio Revio instrument to generate CCS reads containing 5mC and kinetic data
511 for prediction of 6mA via Fibertools(*58*). The FIRE pipeline was then used to obtain haplotype-
512 level accessibility for all samples.
513
514 *Histone CUT&Tag on CD34+ HSPCs and AML samples*
515 Histone profiling used a CUT&Tag-direct protocol(*59*) with modifications relating to cryo-
516 preserved primary AML cells and the release of tagmented DNA from Concanavalin A coated
517 (Con-A) magnetic beads. Cryopreserved HSPC and AML cells were thawed at 37°C, washed
518 once in cold PBS, then pelleted for 3 minutes at 600g and resuspended in hypotonic NE1 buffer

519 (20 mM HEPES-KOH pH 7.9, 10 mM KCl, 0.5 mM spermidine, 10% Triton X-100 and 20%
520 glycerol) followed by incubation on ice for between 45 seconds and 2 minutes for nuclei
521 extraction. The mixture was pelleted for 4 minutes at 1,300g, resuspended in 1× PBS and nuclei
522 were counted using the Trypan blue staining or a ViCell Automated Cell Counter (Beckman
523 Coulter). CUT&Tag-Direct was then carried out as previously described
524 (https://doi.org/10.17504/protocols.io.bcuhiwt6). In brief, nuclei were bound to washed
525 paramagnetic concanavalin A (ConA) beads (Bangs Laboratories) at a concentration of 5 µL
526 washed beads per 50K nuclei and incubated with primary antibody (H3K27me3: Cell Signaling
527 9733S, H3K4me3: Millipore CS200580) at 4°C overnight in Wash Buffer (10 mM HEPES pH
528 7.5, 150 mM NaCl, 0.5 mM spermidine and Roche Complete Protease Inhibitor Cocktail) with
529 2 mM EDTA. Bound nuclei were washed and incubated with 1:100 secondary antibody for
530 1 hour at room temperature and then washed 2x and incubated in Wash-300 Buffer (Wash Buffer
531 with 300 mM NaCl) with 1:50 5 µM loaded pA–Tn5 for 1 hour at room temperature. Nuclei
532 were washed 2x and tagmented in Wash-300 Buffer with 10 mM MgCl2 for 1 hour at 37 °C and
533 then resuspended sequentially in 50 µl of 10 mM TAPS and 5 µl of 10 mM TAPS with 0.1% SDS
534 and incubated for 1 hour at 58 °C. The resulting suspension was mixed well with 16 µl of
535 0.9375% Triton X-100, and then 2 µL each of F and R primers and 25 µL 2× NEBNext Master
536 Mix (New England Biolabs) were added for direct amplification with the following conditions:
537 (1) 58 °C for 5 minutes, (2) 72 °C for 5 minutes, (3) 98 °C for 30 seconds, (4) 98 °C 15 seconds,
538 (5) 60 °C for 15 seconds, (6) repeat steps 4–5 13 times, (7) 72 °C for 1 minute and (8) hold at
539 8 °C. DNA from amplified product was purified via AMPure bead cleanup and resuspended in
540 25 µl of 10 mM Tris-HCl with 1 mM EDTA. Libraries were assessed using the Qubit (Thermo
541 Fisher Scientific) and TapeStation (Agilent) systems and sequencing was performed on an

542 Illumina NovaSeq Xplus to obtain a minimum of 2 million 2x150 bp paired end reads. All data
543 were analyzed via the nf-core(*60*) CUT&Run analysis pipeline to obtain normalized signal in
544 bigwig format.
545
546 *Bulk RNAseq on AML samples and HSC clones*
547 RNA was extracted from 10^6 cells using QIAquick RNA micro kit (Zymo Research). RNA
548 integrity was assessed by RIN scores by Agilent TapeStation 4150 (Agilent Technologies).
549 Quantification of RNA eluates obtained by Qubit RNA BR Assay kit (Invitrogen-Thermo-
550 Fisher). RNAseq libraries were generated via rRNA/Globin HMR depletion followed by
551 ligation-based library preparation (Watchmaker Genomics). Libraries were assessed using
552 Agilent TapeStation 4150 with High Sensitivity D1000 screen tapes (Agilent Technologies) and
553 Qubit dsDNA HS Assays (Invitrogen-Thermo-Fisher). Sequencing was performed on Illumina
554 NovaSeq Xplus to obtain a minimum of 50 million paired end 2x150 bp reads. Data processing
555 used the Illumina DRAGEN RNA pipeline to obtain normalized gene and transcript-level
556 expression values in transcripts per million (TPM).
557
558 *Differentially methylated region (DMR) identification from WGBS data*
559 The DSS(*61*) and bsseq(*62*) packages in R (version 4.3) were used to identify DMRs between
560 each AML sample (N=100) and 17 normal hematopoietic cell methylation datasets (9 CD34+
561 HSPC samples, 3 promyelocyte samples, 3 neutrophil samples, and 2 monocyte samples, all
562 purified as described above from normal bone marrow aspirates from adults aged 20-50). An
563 FDR cutoff of 0.05 and minimum methylation difference of 0.3 were used within DSS without
564 additional filtering. Analysis of DMR recurrence used *bedtools*(*63*) to merge all DMRs and count

overlaps with the DMR set from each AML sample; initial merging and overlapping operations used default settings with no minimum overlap. DMR hotspots were then defined using *bedtools multiintersect* to obtain intervals that had >=25 overlapping DMRs across the 100 AML samples and had at least 5 CpG. Coverage-weighted mean methylation of all 'multi-intersect' DMRs was calculated for each AML sample and the pooled normal hematopoietic cell data using *methfast*, a custom c program for aggregating CpG methylation counts over bed intervals (code available upon request). These unmanipulated methylation fractions were used for all figures, statistical calculations, and comparisons, except for the heatmaps in Figure 1E where smoothing was performed to impute missing data for visualization (smoothed values were not used for sorting or determining methylation levels).

DNA fragment-level and allele-specific methylation analysis from WGBS data

Fragment-level methylation metrics were calculated in private and recurrent DMRs using all normal hematopoietic cell datasets using mHapSuite(*38*). Allele-specific methylation (ASM) analysis was performed by first identifying common single-nucleotide polymorphisms (SNPs) from the 1000 Genomes Project (1000G_phase1.snps.high_confidence.hg38.vcf.gz) that overlapped with IMR hotspots. Sequencing aligned reads covering these "hotspot SNPs" were then partitioned into two groups: those matching the reference allele and those matching the specific alternate allele defined in the 1000 Genomes Project. For the subsequent analysis of an IMR hotspot in an individual sample, each allele group was required to have a minimum of 8 reads, with each read spanning at least 4 CpGs. Individual reads were classified as methylated (≥70% of CpGs methylated) or unmethylated (≤30% of CpGs methylated); reads falling between these thresholds were designated "undetermined". Finally, Fisher's exact test was used to

588 compare the number of methylated and unmethylated reads between the reference and alternate
589 allele groups at each IMR hotspot. P-values were adjusted for multiple testing using the
590 Benjamini-Hochberg method, and hotspots with an FDR < 0.05 were considered significant
591 ASM sites. The code used for this analysis is available at https://github.com/dhslab/methtools.
592
593 *ASM analysis from ONT data*
594 ASM regions were identified from ONT data by first importing haplotype-resolved 5mC counts
595 into *bsseq* objects in R and then calling DMRs between haplotypes with *DSS* using a minimum
596 FDR of 0.05 and methylation difference of 0.4. ASM regions were then further filtered to
597 exclude intervals meeting any of the following criteria: 1) on the X or Y chromosome, 2)
598 overlaps a known imprinted region (N=782, from (*64*, *65*)), 3) occurs within 1,000 bp of an
599 identified structural variant in the ONT data, or 4) overlaps a 10,000 bp region with a SNP
600 density that is in the top 1% across the genome.
601
602 *Identification and analysis of IMR blocks in ONT data from normal HSPCs and AML samples*
603 To define IMR blocks we pooled three sets of genomic coordinates: DMR hotspots from our
604 AML WGBS data, ASM regions from our AML ONT data, and known IMRs in normal
605 tissues(*37*). Coordinates from these sources were merged to create a unified set of intervals.
606 Within these intervals, we identified methylation haplotype blocks (MHBs) by adapting a
607 previously described method(*40*) for long read ONT data. Specifically, per-read CpG
608 methylation calls were extracted from the ONT BAM files of four normal donors and 10 AML
609 samples using modkit (https://github.com/nanoporetech/modkit). From this read-level
610 methylation data, we calculated the methylation linkage disequilibrium (mLD) between adjacent

611 CpG sites, measured as the squared Pearson correlation coefficient (r^2), requiring a minimum of
612 10 reads covering a CpG pair for the calculation. An MHB was then defined as a contiguous
613 region containing at least four consecutive CpG sites where the r^2 value between any two
614 adjacent CpGs was ≥ 0.5. The code used for this analysis is available at
615 https://github.com/dhslab/methtools. To identify allele-specific methylation (ASM) and
616 epimutations within IMR blocks using ONT data, we applied Fisher's exact test. For the ASM
617 analysis, we compared the counts of methylated and unmethylated CpGs between the two
618 haplotypes. For the epimutation analysis, we compared the aggregated counts of methylated and
619 unmethylated CpGs (regardless of haplotype) between AML or HSC samples (for data from
620 expanded HSC bulk cells and clones) and pooled HSPCs from normal donors (n=4). For a block
621 to be included, we required a minimum of four covered CpGs. Furthermore, we mandated a
622 minimum adjusted CpG coverage (defined as total CpG counts divided by the number of CpGs
623 in the block) of 5 per haplotype for ASM and 5 per sample for epimutation. P-values for both
624 analyses were adjusted for multiple testing using the Benjamini-Hochberg method across all
625 evaluable blocks. A significant ASM call was defined by an FDR < 0.05 and an absolute
626 methylation difference between haplotypes > 0.4. A significant epimutation was defined by an
627 FDR < 0.05 and an absolute methylation difference between the test and normal samples > 0.3.
628
629 *Histone analysis at IMR blocks*
630 Histone analysis at IMR blocks was performed using H3K4me3 and H3K27me3 CUT&Tag data
631 from 7 AML samples and 3 mobilized CD34+ HSPC samples. All analysis used normalized
632 signal from bigwig files produced by the nf-core pipeline. Mean methylation at each block was
633 classified as being intermediate (i.e., having ASM) or being hyper or hypomethylated on both

634 haplotypes. Aggregate normalized signal for each modification in 200 equally spaced bins was
635 then calculated for a 5 kbp window centered on the block location for analysis by methylation-
636 defined groups.
637
638 *Fiber-seq FIRE analysis*
639 Haplotype-resolved chromatin accessibility was assessed using the Fiber-seq Inferred Regulatory
640 Elements (FIRE) analysis pipeline(*66*), available at https://github.com/fiberseq/FIRE. The
641 workflow was run using aligned BAM files as input, and accessibility was quantified as the
642 percentage of accessible fibers per region. Analysis of FIRE signal at IMR blocks used either
643 combined or haplotype-level estimates of percent accessibility and were performed at IMR
644 blocks grouped by methylation status (see histone analysis above).
645
646 *Short read genome and exome sequencing of AML samples*
647 Whole-genome sequencing (WGS) was performed on representation and relapse AML samples
648 from patients 112200, 627311, and 895870 with matched normal tissue from skin biopsies. All
649 sequencing was performed using 500ng of DNA input to generate libraries with the Illumina
650 DNA library preparation kit, which were quantified by qPCR and sequenced to obtain a target
651 genome coverage of 60x in 2x150 bp paired end reads on an Illumina NovaSeq Xplus sequencer.
652 Data were analyzed using paired somatic mode with the Illumina DRAGEN software. Identified
653 somatic variants were filtered to retain single nucleotide variants with PASS filter flag and total
654 coverage between 20x and 90x to minimize sequencing artifacts. Whole-exome data for the
655 remission samples was described previously(*42*); variants and their associated variant allele
656 fractions were used directly from that publication.

657

658 *IMR block identification in WGBS from normal tissues*

659 To identify IMR blocks in normal tissues (brain, lung, colon, breast, and pancreas), we began
660 with a set of previously defined regions of bimodal methylation "bimodal blocks" from WGBS
661 data(*44*). We then applied a multi-step filtering process to refine these regions and isolate those
662 specific to a single tissue type. First, to ensure consistency within a given tissue, we only
663 retained bimodal blocks that were present in all normal samples for each tissue type. Next, these
664 consistent blocks from all tissue types were merged to create a non-redundant block list
665 (minimum block size of 50 bp; minimum distance between blocks of 50 bp). To isolate truly
666 tissue-specific blocks and exclude germline imprinted regions, this non-redundant list was
667 subjected to a second round of filtering. For each block, we calculated the average methylation
668 within its matched-tissue samples and the average methylation across all other (non-matched)
669 normal samples. A block was kept only if it exhibited intermediate methylation specifically in its
670 matched tissue, defined by two criteria: 1) an average methylation level between 0.3 and 0.7 with
671 a coefficient of variation (CV) ≤ 0.5 within the matched tissue, and 2) an absolute difference in
672 average methylation of ≥ 0.2 between the matched and non-matched tissues. This process
673 resulted in a final set of tissue-specific IMR blocks in hg19 coordinates. For compatibility with
674 the solid-tumor ONT data, a second version of these block coordinates was generated in hg38
675 using liftOver.

676

677 *Analysis of IMR blocks and other regions in WGBS and ONT data from solid tumors*

678 To analyze methylation patterns in solid tumor WGBS and ONT data, we first defined several
679 sets of genomic regions for analysis. These included the IMR blocks described above, CpG

islands downloaded from the UCSC genome browser, and tissue-specific TSS and enhancers extracted from Roadmap Epigenomics Consortium ChromHMM annotations (model identifiers: E035 for blood, E073 for brain, E096 for lung, E075 for colon, E027 for breast, E098 for pancreas)(*50*). For the tumor methylation data, we used datasets from GEO: GSE121721 (WGBS: brain), GSE212391 (WGBS: other solid tumors), and GSE270257 (ONT: all solid tumors). For the matched normal samples, we downloaded beta value files from the DNA methylation atlas(*45*). All datasets were processed into a unified CpG-level bedmethyl format; for the normal samples, this conversion was performed using wgbstools(*67*). We then used methfast (https://github.com/dhslab/methfast) to aggregate CpG methylation counts from these bedmethyl files over all genomic regions of interest. For the blood cell type analyses, we used the same WGBS and ONT data for normal and AML samples as previously described. In Figure 5 and Figure S5, these normal hematopoietic cells and AML tumor samples are represented as the 'blood' normal and tumor category, respectively. Finally, to identify epimutations (in WGBS and ONT) and ASM (in ONT), we applied the same Fisher's exact test-based approaches used for the hematopoietic cells, which involved comparing aggregated counts between tumor and normal samples for epimutation, and between the two haplotypes for ASM

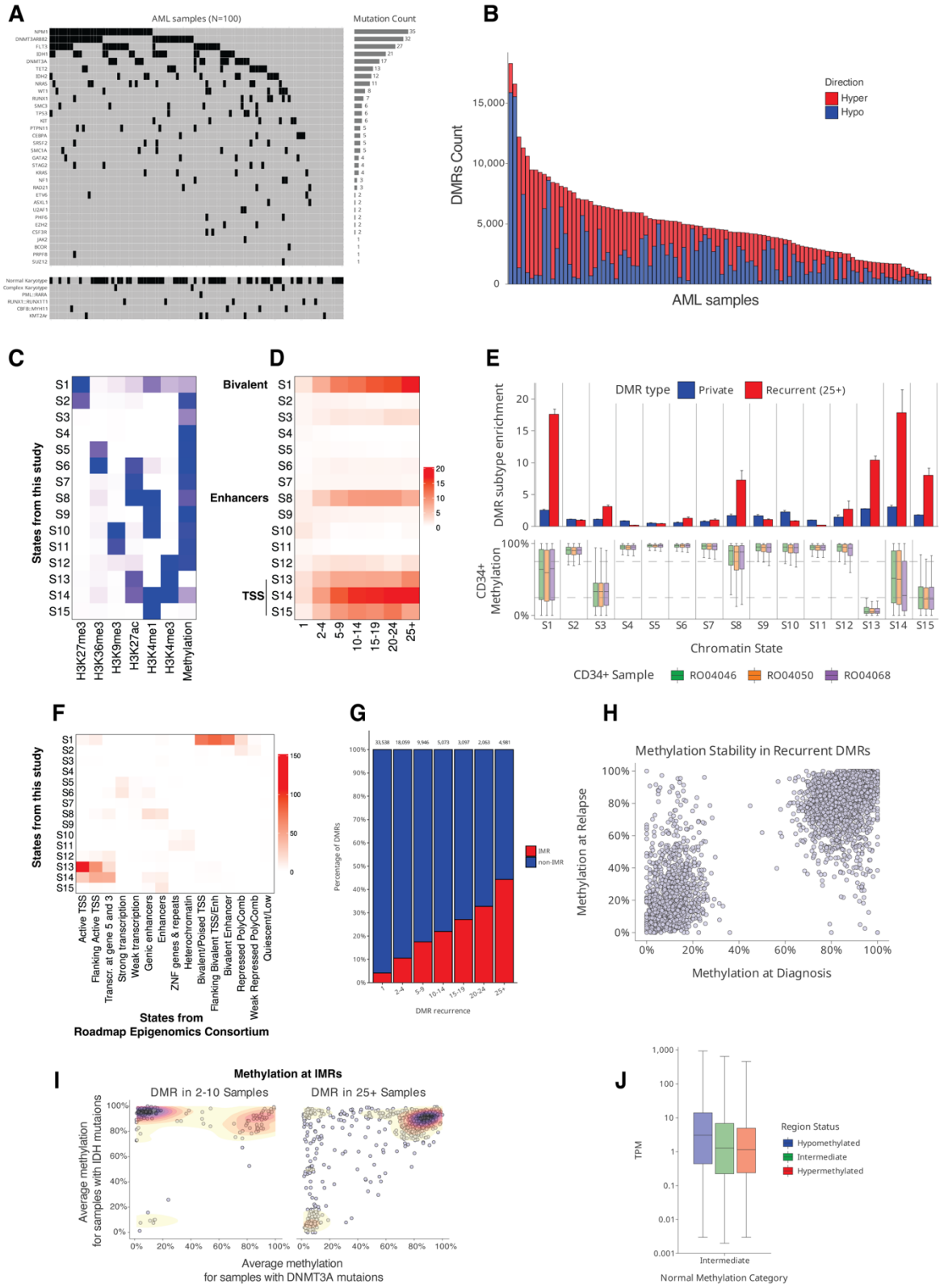
A
AML samples (N=100)
Mutation Count
B
Direction
Hyper
Hypo
DMRs Count
AML samples
C
States from this study
H3K27me3
H3K36me3
H3K9me3
H3K27ac
H3K4me1
H3K4me3
Methylation
D
Bivalent
Enhancers
TSS
E
DMR type
Private
Recurrent (25+)
DMR subtype enrichment
CD34+ Methylation
Chromatin State
CD34+ Sample
RO04046
RO04050
RO04068
F
States from this study
Active TSS
Flanking Active TSS
Transcr. at gene 5 and 3
Strong transcription
Weak transcription
Genic enhancers
Enhancers
ZNF genes & repeats
Heterochromatin
Bivalent/Poised TSS
Flanking Bivalent TSS/Enh
Bivalent Enhancer
Repressed PolyComb
Weak Repressed PolyComb
Quiescent/Low
States from
Roadmap Epigenomics Consortium
G
Percentage of DMRs
DMR recurrence
IMR
non-IMR
H
Methylation Stability in Recurrent DMRs
Methylation at Relapse
Methylation at Diagnosis
I
Methylation at IMRs
DMR in 2-10 Samples
DMR in 25+ Samples
Average methylation
for samples with IDH mutaions
Average methylation
for samples with DNMT3A mutaions
J
TPM
Region Status
Hypomethylated
Intermediate
Hypermethylated
Normal Methylation Category

696

697

Fig. S1. Identification of differentially methylated regions in AML and their enrichment in intermediately methylated regions in normal hematopoietic cells.
(A) Mutation and karyotype status of AML samples used for WGBS analysis. (**B**) Number of DMRs identified in each AML sample compared to CD34+ cells. **(C)** Emission parameters for states S1 through S15 of a chromHMM model trained on six histone modifications (H3K4me1, H3K4me3, H3K27me3, H3K36me3, H3K9me3, and H3K27ac) and DNA methylation data from purified CD34+ HSPCs. (**D**) Heatmap of DMR enrichment grouped by recurrence frequency in chromatin states defined in HSPCs. (**E**) (Top) Relative enrichment of private and recurrent DMRs and (Bottom) Methylation levels in CD34+ (n=3) at chromatin states. For the methylation analysis, all segments within each state are included. (**F**) Heatmap showing the enrichment mapping of predefined functional genomic regions, annotated in published CD34+ data from the Roadmap Epigenomics Consortium (histone modifications only), within the chromatin states (S1-S15) defined in this study using both histone modifications and DNA methylation in CD34+ cells. (**G**) Overlap percentage of AML DMRs (grouped by recurrence frequency) with previously published intermediately methylated regions (IMRs)(*37*). (**H**) Methylation levels at IMR hotspots with altered methylation (DMRs called), identified in the presentation sample, comparing the methylation levels between presentation and relapse samples from the same patient. (**I**) Comparison of average methylation levels between samples with DNMT3A and IDH mutations, including only those with an identified differentially methylated region (DMR). The analysis distinguishes between two categories of normally intermediately methylated regions (IMRs) based on DMR recurrence: high-recurrence hotspots (DMRs in ≥25 samples) and low-recurrence regions (DMRs in 2–10 samples). Only IMRs with at least two differentially methylated samples in each mutation group were included in the comparison. Regions with low recurrence exhibit methylation patterns that appear to be mutation-driven, while highly recurrent regions are consistently hypermethylated or hypomethylated regardless of mutation type. (**J**) RNA expression levels (TPM) of genes with promoters overlapping recurrent IMR hotspots in AML samples, with samples grouped by promoter methylation status into hypomethylated (<30%), intermediately methylated (30–70%), and hypermethylated (>70%) promoter categories. $P < 10^{-8}$ for a difference in expression across these groups, based on an ANOVA.

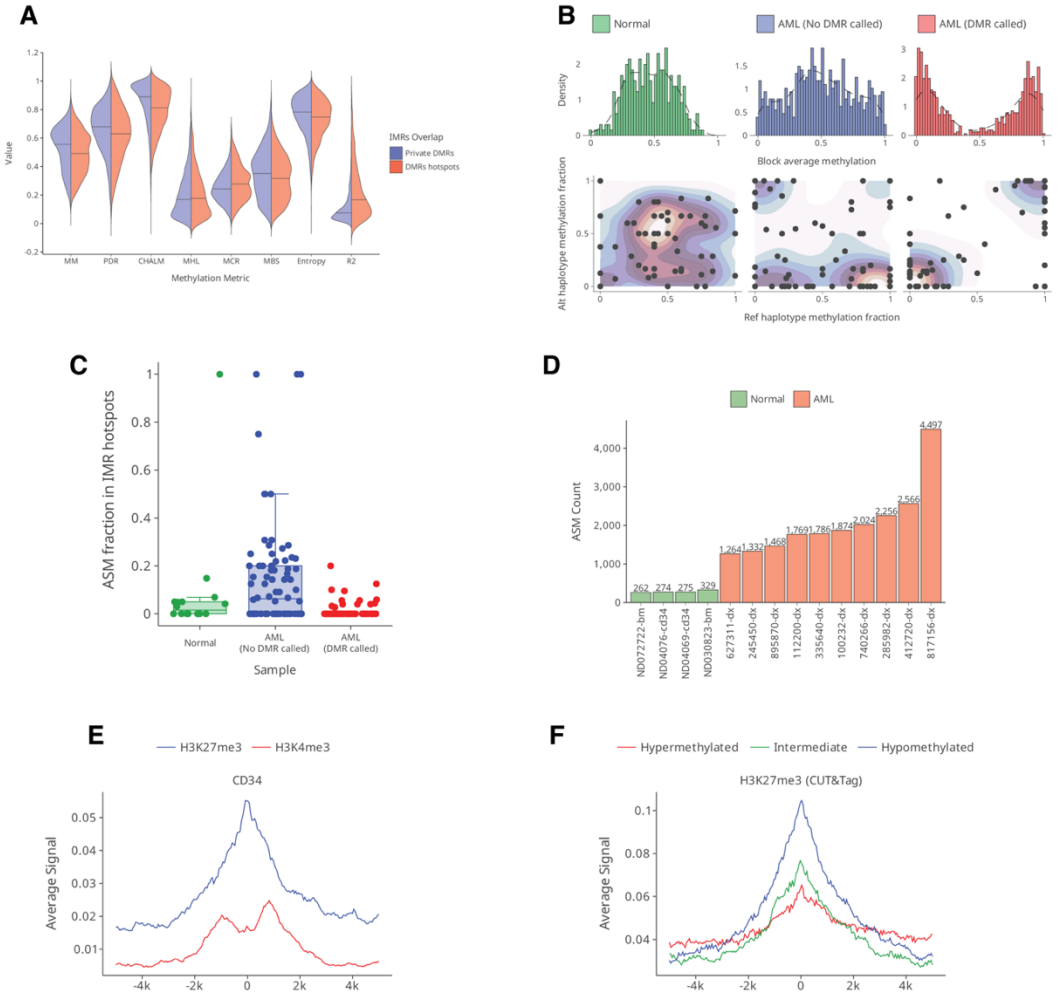

Fig. S2. Intermediately methylated regions in normal hematopoietic cells display allelic methylation patterns in AML. (A) Fragment-level WGBS methylation metrics statistics at IMRs in normal hematopoietic cells, comparing DMR hotspots vs. non-hotspot DMRs. **(B)** Methylation at IMR hotspots in normal hematopoietic cells, AML samples without differential methylation (no DMR called), and AML samples with DMRs (DMR called). Top: distribution histograms of average methylation at IMR hotspots; bottom: scatter plots comparing the average methylation of reference versus alternate haplotypes for each IMR hotspot with phased WGBS reads above the coverage threshold. **(C)** Fraction of IMR hotspots exhibiting allele-specific methylation (ASM) from WGBS in normal hematopoietic cells, AML without DMRs, and AML with DMRs. **(D)** Number of ASM regions identified from ONT haplotype-resolved methylation using the DSS R package in normal hematopoietic cells and AML samples. **(E)** Aggregated CUT&Tag signal for H3K27me3 and H3K4me3 modifications at IMR blocks in normal hematopoietic cells. **(F)** Aggregated H3K27me3 CUT&Tag signal at IMR blocks in AML samples, with blocks grouped by methylation status (hypomethylated, intermediate, or hypermethylated).

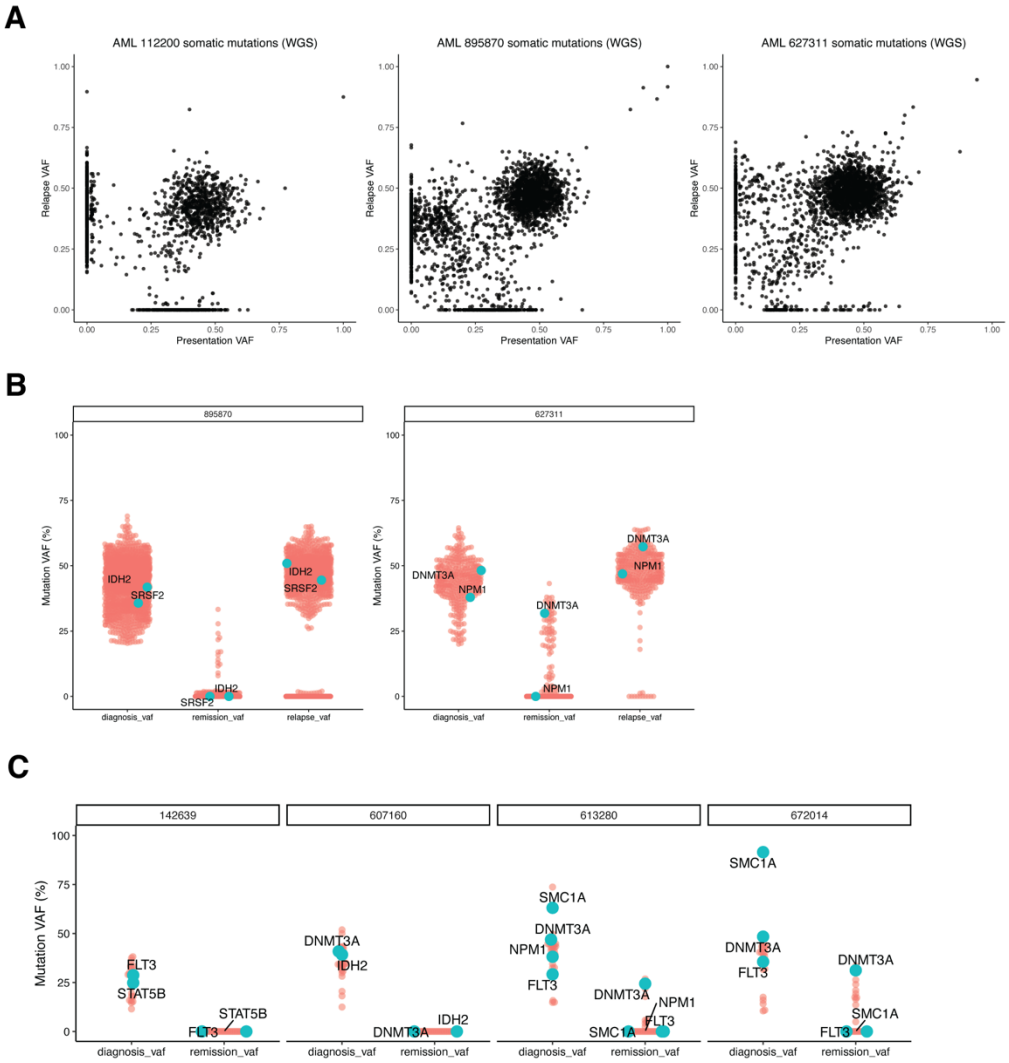

745

746 **Fig. S3. IMR blocks are clonal events in AML and normal hematopoietic cell populations.**
747 **(A)** Somatic mutations from whole-genome sequencing of AML patients 112200, 895870, and
748 627311 at presentation and relapse. Shown are the VAFs at relapse (Y-axis) and presentation (X-
749 axis) demonstrating their clonal relationships. **(B)** VAFs for somatic mutations from AML patient
750 895870 with nearly complete clearance of all variants in remission (left) vs. AML patient 627311
751 who had persistent variants, including *DNMT3A*^{R729W}, indicating clonal hematopoiesis at the
752 remission timepoint. Both patients had *de novo* AML and were treated with standard "7+3"
753 induction chemotherapy and were in complete morphologic remission at the remission time
754 point. **(C)** Mutation clearance plots from whole-exome sequencing of 4 additional AML patients
755 who achieved a complete morphologic remission after induction chemotherapy(*42*) .
756

757

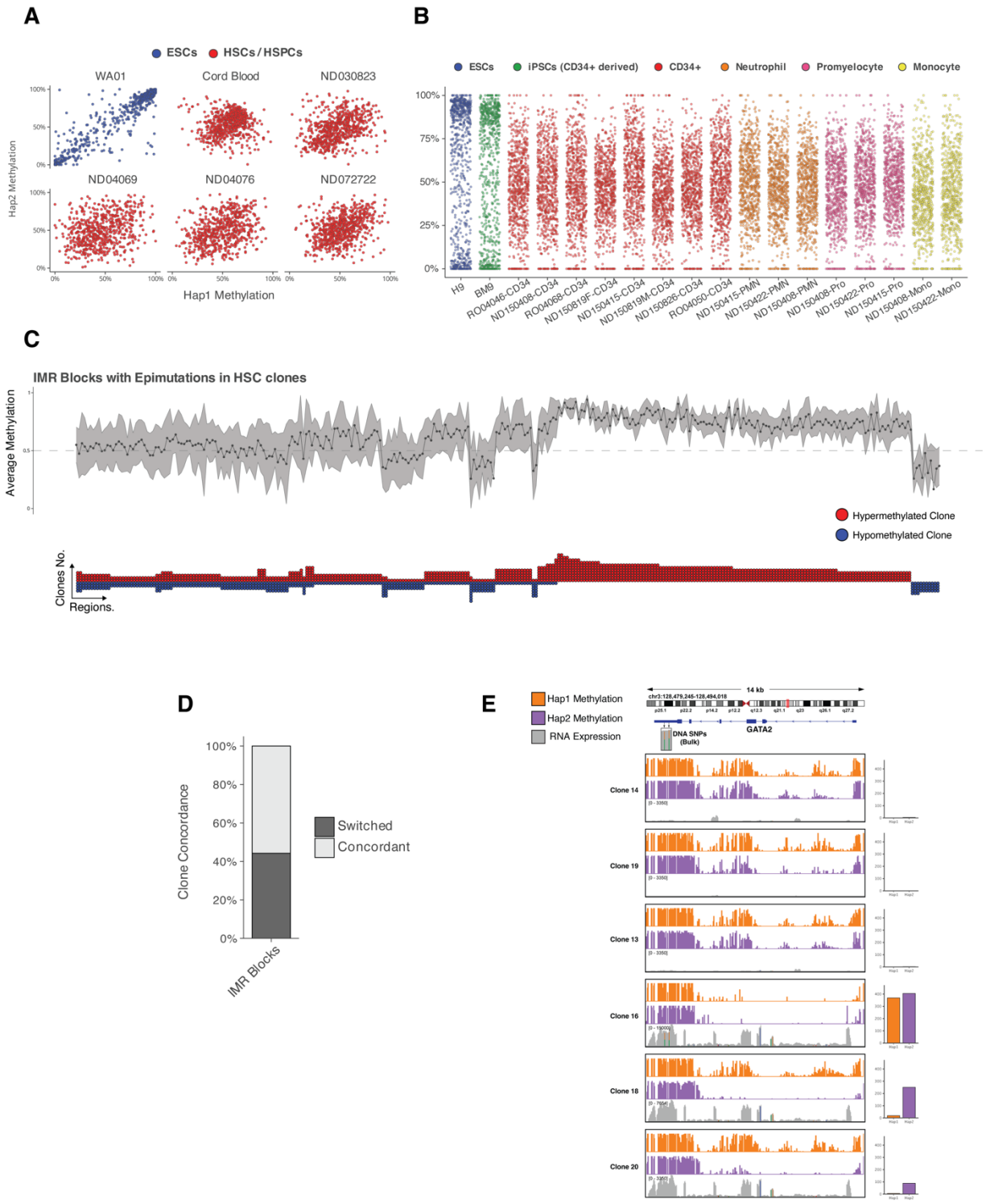
A
ESCs
HSCs / HSPCs
WA01
Cord Blood
ND030823
ND04069
ND04076
ND072722
Hap2 Methylation
Hap1 Methylation
B
ESCs
iPSCs (CD34+ derived)
CD34+
Neutrophil
Promyelocyte
Monocyte
H9
BM9
RO04046-CD34
ND150408-CD34
RO04068-CD34
ND150819F-CD34
ND150415-CD34
ND150819M-CD34
ND150826-CD34
RO04050-CD34
ND150415-PMN
ND150422-PMN
ND150408-PMN
ND150408-Pro
ND150422-Pro
ND150415-Pro
ND150408-Mono
ND150422-Mono
C
IMR Blocks with Epimutations in HSC clones
Average Methylation
Hypermethylated Clone
Hypomethylated Clone
Clones No.
Regions.
D
Clone Concordance
Switched
Concordant
IMR Blocks
E
Hap1 Methylation
Hap2 Methylation
RNA Expression
14 kb
GATA2
DNA SNPs (Bulk)
Clone 14
Clone 19
Clone 13
Clone 16
Clone 18
Clone 20

758

759

760 **Fig. S4. Random allele-specific methylation at IMR blocks is established in single**
761 **hematopoietic stem cells and is associated with allele-specific gene expression. (A)**
762 Comparison of haplotype 1 versus haplotype 2 ONT methylation at IMR blocks with
763 intermediate methylation in bulk HSCs. Scatter plots are shown for WA01 embryonic stem cells
764 (ESCs), cord blood HSCs, and normal donor hematopoietic stem and progenitor cells (HSPCs).
765 **(B)** Average WGBS methylation levels at IMR blocks for H9 embryonic stem cells (ESCs), BM9
766 induced pluripotent stem cells (iPSCs) derived from CD34+ cells, CD34+ cells, and
767 differentiated myeloid lineages. Each point represents the non-phased average WGBS
768 methylation at a single single IMR for the indicated sample. **(C)** Analysis of epimutations in
769 single HSC clones at IMR blocks with intermediate methylation. The top line plot displays the
770 average methylation across all clones for each block. The dot plot below indicates individual
771 clones exhibiting either hyper-methylation (red) or hypo-methylation (blue) epimutations at these
772 blocks relative to normal HSPCs. Only IMR blocks with epimutations observed in at least four
773 clones were included in this analysis. **(D)** Bar plot quantifying the concordance of epimutation
774 type across clones for the IMR blocks shown in (C). "Switched" indicates regions where both
775 hyper- and hypo-methylation events were observed in different clones, while "Concordant"
776 indicates regions where all observed epimutations were of the same type. **(E)** Allele-specific
777 methylation is associated with allele-specific expression at the *GATA2* locus. Tracks for
778 representative single HSC clones show Haplotype 1 methylation (orange), Haplotype 2
779 methylation (purple), and RNA expression coverage (grey), with two heterozygous SNPs in the
780 last exon used for phasing RNA expression. The bar plots on the right quantify haplotype-
781 specific expression (TPM).
782

783

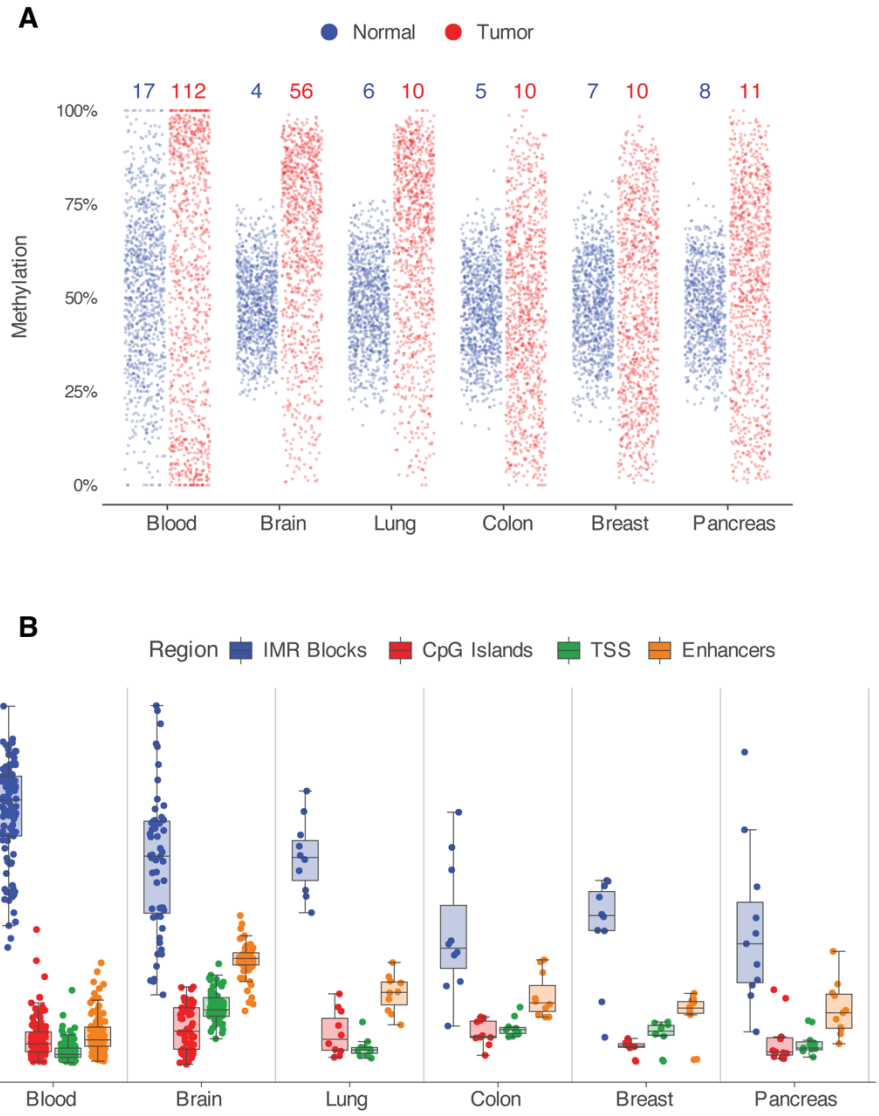

Fig. S5. Epimutations at tissue-specific IMRs using WGBS cancer datasets. (A) Distribution of average methylation levels at tissue-specific IMRs in normal tissues (blue) and their corresponding primary tumors (red), based on WGBS data. The numbers at the top of the plot indicate the number of samples included in each group. Each point represents the average methylation at a single IMR block within a sample. For visualization, 1,000 points were randomly sampled for each group. **(B)** Percentage of various genomic features exhibiting epimutations across different cancer types, based on WGBS data. The box plots compare the percentage of

epimutations within tissue-specific IMRs (IMR Blocks), CpG islands, tissue-specific transcription start sites (TSS), and tissue-specific enhancers. Each point represents an individual tumor sample.

References and Notes:

1. A. P. Feinberg, B. Vogelstein, Hypomethylation distinguishes genes of some human cancers from their normal counterparts. *Nature* **301**, 89–92 (1983).
2. A. P. Feinberg, B. Vogelstein, Hypomethylation of ras oncogenes in primary human cancers. *Biochem Bioph Res Co* **111**, 47–54 (1983).
3. M. A. Gama-Sosa, V. A. Slagel, R. W. Trewyn, R. Oxenhandler, K. C. Kuo, C. W. Gehrke, M. Ehrlich, The 5-methylcytosine content of DNA from human tumors. *Nucleic Acids Res.* **11**, 6883–6894 (1983).
4. D. H. Spencer, D. A. Russler-Germain, S. Ketkar, N. M. Helton, T. L. Lamprecht, R. S. Fulton, C. C. Fronick, M. O'Laughlin, S. E. Heath, M. Shinawi, P. Westervelt, J. E. Payton, L. D. Wartman, J. S. Welch, R. K. Wilson, M. J. Walter, D. C. Link, J. F. DiPersio, T. J. Ley, CpG Island Hypermethylation Mediated by DNMT3A Is a Consequence of AML Progression. *Cell* **168**, 801-816.e13 (2017).
5. E. R. Wilson, N. M. Helton, S. E. Heath, R. S. Fulton, J. E. Payton, J. S. Welch, M. J. Walter, P. Westervelt, J. F. DiPersio, D. C. Link, C. A. Miller, T. J. Ley, D. H. Spencer, Focal disruption of DNA methylation dynamics at enhancers in IDH-mutant AML cells. *Leukemia* **36**, 935–945 (2022).
6. J. L. Glass, D. Hassane, B. J. Wouters, H. Kunimoto, R. Avellino, F. E. Garrett-Bakelman, O. A. Guryanova, R. Bowman, S. Redlich, A. M. Intlekofer, C. Meydan, T. Qin, M. Fall, A. Alonso, M. L. Guzman, P. J. M. Valk, C. B. Thompson, R. Levine, O. Elemento, R. Delwel, A. Melnick, M. E. Figueroa, Epigenetic Identity in AML Depends on Disruption of Nonpromoter Regulatory Elements and Is Affected by Antagonistic Effects of Mutations in Epigenetic Modifiers. *Cancer Discov* **7**, 868–883 (2017).
7. D. Capper, D. T. W. Jones, M. Sill, V. Hovestadt, D. Schrimpf, D. Sturm, C. Koelsche, F. Sahm, L. Chavez, D. E. Reuss, A. Kratz, A. K. Wefers, K. Huang, K. W. Pajtler, L. Schweizer, D. Stichel, A. Olar, N. W. Engel, K. Lindenberg, P. N. Harter, A. K. Braczynski, K. H. Plate, H. Dohmen, B. K. Garvalov, R. Coras, A. Hölsken, E. Hewer, M. Bewerunge-Hudler, M. Schick, R. Fischer, R. Beschorner, J. Schittenhelm, O. Staszewski, K. Wani, P. Varlet, M. Pages, P. Temming, D. Lohmann, F. Selt, H. Witt, T. Milde, O. Witt, E. Aronica, F. Giangaspero, E. Rushing, W. Scheurlen, C. Geisenberger, F. J. Rodriguez, A. Becker, M. Preusser, C. Haberler, R. Bjerkvig, J. Cryan, M. Farrell, M. Deckert, J. Hench, S. Frank, J. Serrano, K. Kannan, A. Tsirigos, W. Brück, S. Hofer, S. Brehmer, M. Seiz-Rosenhagen, D. Hänggi, V. Hans, S. Rozsnoki, J. R. Hansford, P. Kohlhof, B. W. Kristensen, M. Lechner, B. Lopes, C. Mawrin, R. Ketter, A. Kulozik, Z. Khatib, F. Heppner, A. Koch, A. Jouvet, C. Keohane, H. Mühleisen, W. Mueller, U. Pohl, M. Prinz, A. Benner, M. Zapatka, N. G. Gottardo, P. H. Driever, C. M. Kramm, H. L. Müller, S. Rutkowski, K. von Hoff, M. C. Frühwald, A. Gnekow, G. Fleischhack, S. Tippelt, G. Calaminus, C.-M. Monoranu, A. Perry, C. Jones, T. S. Jacques, B. Radlwimmer, M. Gessi, T. Pietsch, J. Schramm, G. Schackert, M. Westphal, G. Reifenberger, P. Wesseling, M. Weller, V. P. Collins, I. Blümcke, M. Bendszus, J. Debus, A. Huang, N.

Jabado, P. A. Northcott, W. Paulus, A. Gajjar, G. W. Robinson, M. D. Taylor, Z. Jaunmuktane, M. Ryzhova, M. Platten, A. Unterberg, W. Wick, M. A. Karajannis, M. Mittelbronn, T. Acker, C. Hartmann, K. Aldape, U. Schüller, R. Buslei, P. Lichter, M. Kool, C. Herold-Mende, D. W. Ellison, M. Hasselblatt, M. Snuderl, S. Brandner, A. Korshunov, A. von Deimling, S. M. Pfister, DNA methylation-based classification of central nervous system tumours. *Nature* **555**, 469–474 (2018).

8. C. Koelsche, D. Schrimpf, D. Stichel, M. Sill, F. Sahm, D. E. Reuss, M. Blattner, B. Worst, C. E. Heilig, K. Beck, P. Horak, S. Kreutzfeldt, E. Paff, S. Stark, P. Johann, F. Selt, J. Ecker, D. Sturm, K. W. Pajtler, A. Reinhardt, A. K. Wefers, P. Sievers, A. Ebrahimi, A. Suwala, F. Fernández-Klett, B. Casalini, A. Korshunov, V. Hovestadt, F. K. F. Kommoss, M. Kriegsmann, M. Schick, M. Bewerunge-Hudler, T. Milde, O. Witt, A. E. Kulozik, M. Kool, L. Romero-Pérez, T. G. P. Grünewald, T. Kirchner, W. Wick, M. Platten, A. Unterberg, M. Uhl, A. Abdollahi, J. Debus, B. Lehner, C. Thomas, M. Hasselblatt, W. Paulus, C. Hartmann, O. Staszewski, M. Prinz, J. Hench, S. Frank, Y. M. H. Versleijen-Jonkers, M. E. Weidema, T. Mentzel, K. Griewank, E. de Álava, J. D. Martín, M. A. I. Gastearena, K. T.-E. Chang, S. Y. Y. Low, A. Cuevas-Bourdier, M. Mittelbronn, M. Mynarek, S. Rutkowski, U. Schüller, V. F. Mautner, J. Schittenhelm, J. Serrano, M. Snuderl, R. Büttner, T. Klingebiel, R. Buslei, M. Gessler, P. Wesseling, W. N. M. Dinjens, S. Brandner, Z. Jaunmuktane, I. Lyskjær, P. Schirmacher, A. Stenzinger, B. Brors, H. Glimm, C. Heining, O. M. Tirado, M. Sáinz-Jaspeado, J. Mora, J. Alonso, X. G. del Muro, S. Moran, M. Esteller, J. K. Benhamida, M. Ladanyi, E. Wardelmann, C. Antonescu, A. Flanagan, U. Dirksen, P. Hohenberger, D. Baumhoer, W. Hartmann, C. Vokuhl, U. Flucke, I. Petersen, G. Mechtersheimer, D. Capper, D. T. W. Jones, S. Fröhling, S. M. Pfister, A. von Deimling, Sarcoma classification by DNA methylation profiling. *Nat. Commun.* **12**, 498 (2021).
9. B. Giacopelli, M. Wang, A. Cleary, Y.-Z. Wu, A. R. Schultz, M. Schmutz, J. S. Blachly, A.-K. Eisfeld, B. Mundy-Bosse, S. Vosberg, P. A. Greif, R. Claus, L. Bullinger, R. Garzon, K. R. Coombes, C. D. Bloomfield, B. J. Druker, J. W. Tyner, J. C. Byrd, C. C. Oakes, DNA methylation epitypes highlight underlying developmental and disease pathways in acute myeloid leukemia. *Genome Res* **31**, gr.269233.120 (2021).
10. S. Baylin, T. H. Bestor, Altered methylation patterns in cancer cell genomes: Cause or consequence? *Cancer Cell* **1**, 299–305 (2002).
11. M. P. Hitchins, Constitutional epimutation as a mechanism for cancer causality and heritability? *Nat. Rev. Cancer* **15**, 625–634 (2015).
12. B. Horsthemke, Heritable germline epimutations in humans. *Nat. Genet.* **39**, 573–574 (2007).
13. R. L. Poole, L. E. Docherty, A. A. Sayegh, A. Caliebe, C. Turner, E. Baple, E. Wakeling, L. Harrison, A. Lehmann, I. K. Temple, D. J. G. Mackay, O. behalf of the I. C. I. Consortium, Targeted methylation testing of a patient cohort broadens the epigenetic and clinical description of imprinting disorders. *Am. J. Méd. Genet. Part A* **161**, 2174–2182 (2013).
14. K. Buiting, S. Groß, C. Lich, G. Gillessen-Kaesbach, O. El-Maarri, B. Horsthemke, Epimutations in Prader-Willi and Angelman Syndromes: A Molecular Study of 136 Patients with an Imprinting Defect. *Am. J. Hum. Genet.* **72**, 571–577 (2003).
15. M. P. Hitchins, R. L. Ward, Constitutional (germline) MLH1 epimutation as an aetiological mechanism for hereditary non-polyposis colorectal cancer. *J. Méd. Genet.* **46**, 793 (2009).
16. C. M. Suter, D. I. K. Martin, R. L. Ward, Germline epimutation of MLH1 in individuals with multiple cancers. *Nat. Genet.* **36**, 497–501 (2004).

17. R. Mulet-Lazaro, S. van Herk, C. Erpelinck, E. Bindels, M. A. Sanders, C. Vermeulen, I. Renkens, P. Valk, A. M. Melnick, J. de Ridder, M. Rehli, C. Gebhard, R. Delwel, B. J. Wouters, Allele-specific expression of GATA2 due to epigenetic dysregulation in CEBPA double-mutant AML. *Blood* **138**, 160–177 (2021).
18. S. B. Simpkins, T. Bocker, E. M. Swisher, D. G. Mutch, D. J. Gersell, A. J. Kovatich, J. P. Palazzo, R. Fishel, P. J. Goodfellow, MLH1 Promoter Methylation and Gene Silencing is the Primary Cause of Microsatellite Instability in Sporadic Endometrial Cancers. *Hum. Mol. Genet.* **8**, 661–666 (1999).
19. K. O'Neill, E. Pleasance, J. Fan, V. Akbari, G. Chang, K. Dixon, V. Csizmok, S. MacLennan, V. Porter, A. Galbraith, C. J. Grisdale, L. Culibrk, J. H. Dupuis, R. Corbett, J. Hopkins, R. Bowlby, P. Pandoh, D. E. Smailus, D. Cheng, T. Wong, C. Frey, Y. Shen, L. F. Paulin, F. J. Sedlazeck, J. M. T. Nelson, E. Chuah, K. L. Mungall, R. A. Moore, R. Coope, A. J. Mungall, M. K. McConechy, L. M. Williamson, K. A. Schrader, S. Yip, M. A. Marra, J. Laskin, S. J. M. Jones, Long-read sequencing of an advanced cancer cohort resolves rearrangements, unravels haplotypes, and reveals methylation landscapes. *medRxiv*, 2024.02.20.24302959 (2024).
20. A. Gimelbrant, J. N. Hutchinson, B. R. Thompson, A. Chess, Widespread Monoallelic Expression on Human Autosomes. *Science* **318**, 1136–1140 (2007).
21. O. Stewart, C. Gruber, H. E. Randolph, R. Patel, M. Ramba, E. Calzoni, L. H. Huang, J. Levy, S. Buta, A. Lee, C. Sazeides, Z. Prue, D. P. H. van Konijnenburg, I. K. Chinn, L. A. Pedroza, J. R. Lupski, E. G. Schmitt, M. A. Cooper, A. Puel, X. Peng, S. Boisson-Dupuis, J. Bustamante, S. Okada, M. Martin-Fernandez, J. S. Orange, J.-L. Casanova, J. D. Milner, D. Bogunovic, Monoallelic expression can govern penetrance of inborn errors of immunity. *Nature*, 1–12 (2025).
22. A. F. A. Seraihi, A. Rio-Machin, K. Tawana, C. Bödör, J. Wang, A. Nagano, J. A. Heward, S. Iqbal, S. Best, N. Lea, D. McLornan, E. J. Kozyra, M. W. Wlodarski, C. M. Niemeyer, H. Scott, C. Hahn, A. Ellison, H. Tummala, S. R. Cardoso, T. Vulliamy, I. Dokal, T. Butler, M. Smith, J. Cavenagh, J. Fitzgibbon, GATA2 monoallelic expression underlies reduced penetrance in inherited GATA2-mutated MDS/AML. *Leukemia* **32**, 2502–2507 (2018).
23. L. Marion-Poll, B. Forêt, D. Zielinski, F. Massip, M. Attia, A. C. Carter, L. Syx, H. Y. Chang, A.-V. Gendrel, E. Heard, Locus specific epigenetic modalities of random allelic expression imbalance. *Nat. Commun.* **12**, 5330 (2021).
24. Q. Deng, D. Ramsköld, B. Reinius, R. Sandberg, Single-Cell RNA-Seq Reveals Dynamic, Random Monoallelic Gene Expression in Mammalian Cells. *Science* **343**, 193–196 (2014).
25. H. Noushmehr, D. J. Weisenberger, K. Diefes, H. S. Phillips, K. Pujara, B. P. Berman, F. Pan, C. E. Pelloski, E. P. Sulman, K. P. Bhat, R. G. W. Verhaak, K. A. Hoadley, D. N. Hayes, C. M. Perou, H. K. Schmidt, L. Ding, R. K. Wilson, D. V. D. Berg, H. Shen, H. Bengtsson, P. Neuvial, L. M. Cope, J. Buckley, J. G. Herman, S. B. Baylin, P. W. Laird, K. Aldape, T. C. G. A. R. Network, Identification of a CpG Island Methylator Phenotype that Defines a Distinct Subgroup of Glioma. *Cancer Cell* **17**, 510–522 (2010).
26. T. J. Ley, C. Miller, L. Ding, B. J. Raphael, A. J. Mungall, A. G. Robertson, K. Hoadley, T. J. Triche, P. W. Laird, J. D. Baty, L. L. Fulton, R. Fulton, S. E. Heath, J. Kalicki-Veizer, C. Kandoth, J. M. Klco, D. C. Koboldt, K.-L. Kanchi, S. Kulkarni, T. L. Lamprecht, D. E. Larson, L. Lin, C. Lu, M. D. McLellan, J. F. McMichael, J. Payton, H. Schmidt, D. H. Spencer, M. H. Tomasson, J. W. Wallis, L. D. Wartman, M. A. Watson, J. Welch, M. C. Wendl, A. Ally, M. Balasundaram, I. Birol, Y. Butterfield, R. Chiu, A. Chu, E. Chuah, H.-J. Chun, R. Corbett, N. Dhalla, R. Guin, A. He, C. Hirst, M. Hirst, R. A. Holt, S. Jones, A. Karsan, D. Lee, H. I. Li, M.

A. Marra, M. Mayo, R. A. Moore, K. Mungall, J. Parker, E. Pleasance, P. Plettner, J. Schein, D. Stoll, L. Swanson, A. Tam, N. Thiessen, R. Varhol, N. Wye, Y. Zhao, S. Gabriel, G. Getz, C. Sougnez, L. Zou, M. D. M. Leiserson, F. Vandin, H.-T. Wu, F. Applebaum, S. B. Baylin, R. Akbani, B. M. Broom, K. Chen, T. C. Motter, K. Nguyen, J. N. Weinstein, N. Zhang, M. L. Ferguson, C. Adams, A. Black, J. Bowen, J. Gastier-Foster, T. Grossman, T. Lichtenberg, L. Wise, T. Davidsen, J. A. Demchok, K. R. M. Shaw, M. Sheth, H. J. Sofia, L. Yang, J. R. Downing, G. Eley, Genomic and Epigenomic Landscapes of Adult De Novo Acute Myeloid Leukemia. *New Engl J Med* **368**, 2059–2074 (2013).

27. T. Mazor, A. Pankov, B. E. Johnson, C. Hong, E. G. Hamilton, R. J. A. Bell, I. V. Smirnov, G. F. Reis, J. J. Phillips, M. J. Barnes, A. Idbaih, A. Alentorn, J. J. Kloezeman, M. L. M. Lamfers, A. W. Bollen, B. S. Taylor, A. M. Molinaro, A. B. Olshen, S. M. Chang, J. S. Song, J. F. Costello, DNA Methylation and Somatic Mutations Converge on the Cell Cycle and Define Similar Evolutionary Histories in Brain Tumors. *Cancer Cell* **28**, 307–317 (2015).
28. T. C. G. A. R. Network, Comprehensive, Integrative Genomic Analysis of Diffuse Lower-Grade Gliomas. *New Engl J Medicine* **372**, 2481–2498 (2015).
29. M. E. Figueroa, S. Lugthart, Y. Li, C. Erpelinck-Verschueren, X. Deng, P. J. Christos, E. Schifano, J. Booth, W. van Putten, L. Skrabanek, F. Campagne, M. Mazumdar, J. M. Greally, P. J. M. Valk, B. Löwenberg, R. Delwel, A. Melnick, DNA Methylation Signatures Identify Biologically Distinct Subtypes in Acute Myeloid Leukemia. *Cancer Cell* **17**, 13–27 (2010).
30. J. Ernst, M. Kellis, Chromatin-state discovery and genome annotation with ChromHMM. *Nat Protoc* **12**, 2478–2492 (2017).
31. G. Elliott, C. Hong, X. Xing, X. Zhou, D. Li, C. Coarfa, R. J. A. Bell, C. L. Maire, K. L. Ligon, M. Sigaroudinia, P. Gascard, T. D. Tlsty, R. A. Harris, L. C. Schalkwyk, M. Bilenky, J. Mill, P. J. Farnham, M. Kellis, M. A. Marra, A. Milosavljevic, M. Hirst, G. D. Stormo, T. Wang, J. F. Costello, Intermediate DNA methylation is a conserved signature of genome regulation. *Nat. Commun.* **6**, 6363 (2015).
32. Y. Ding, K. Cai, L. Liu, Z. Zhang, X. Zheng, J. Shi, mHapTk: a comprehensive toolkit for the analysis of DNA methylation haplotypes. *Bioinformatics* **38**, 5141–5143 (2022).
33. Y. Feng, Z. Zhang, Y. Hong, Y. Ding, L. Liu, S. Gao, H. Fang, J. Shi, A DNA methylation haplotype block landscape in human tissues and preimplantation embryos reveals regulatory elements defined by comethylation patterns. *Genome Res.* **33**, 2041–2052 (2023).
34. S. Guo, D. Diep, N. Plongthongkum, H.-L. Fung, K. Zhang, K. Zhang, Identification of methylation haplotype blocks aids in deconvolution of heterogeneous tissue samples and tumor tissue-of-origin mapping from plasma DNA. *Nat. Genet.* **49**, 635–642 (2017).
35. A. B. Stergachis, B. M. Debo, E. Haugen, L. S. Churchman, J. A. Stamatoyannopoulos, Single-molecule regulatory architectures captured by chromatin fiber sequencing. *Science* **368**, 1449–1454 (2020).
36. M. J. Slade, R. Ghasemi, M. O'Laughlin, T. Burton, R. S. Fulton, H. J. Abel, E. J. Duncavage, T. J. Ley, M. A. Jacoby, D. H. Spencer, Persistent Molecular Disease in Adult Patients With AML Evaluated With Whole-Exome and Targeted Error-Corrected DNA Sequencing. *JCO Precis. Oncol.* **7**, e2200559 (2023).
37. K. Hu, J. Yu, K. Suknuntha, S. Tian, K. Montgomery, K.-D. Choi, R. Stewart, J. A. Thomson, I. I. Slukvin, Efficient generation of transgene-free induced pluripotent stem cells from normal and neoplastic bone marrow and cord blood mononuclear cells. *Blood* **117**, e109–e119 (2011).
38. V. L. Wilson, P. A. Jones, DNA Methylation Decreases in Aging But Not in Immortal Cells. *Science* **220**, 1055–1057 (1983).

39. J. Rosenski, A. Peretz, J. Magenheim, N. Loyfer, R. Shemer, B. Glaser, Y. Dor, T. Kaplan, Atlas of imprinted and allele-specific DNA methylation in the human body. *Nat. Commun.* **16**, 2141 (2025).
40. N. Loyfer, J. Magenheim, A. Peretz, G. Cann, J. Bredno, A. Klochendler, I. Fox-Fisher, S. Shabi-Porat, M. Hecht, T. Pelet, J. Moss, Z. Drawshy, H. Amini, P. Moradi, S. Nagaraju, D. Bauman, D. Shveiky, S. Porat, U. Dior, G. Rivkin, O. Or, N. Hirshoren, E. Carmon, A. Pikarsky, A. Khalaileh, G. Zamir, R. Grinbaum, M. A. Gazala, I. Mizrahi, N. Shussman, A. Korach, O. Wald, U. Izhar, E. Erez, V. Yutkin, Y. Samet, D. R. Golinkin, K. L. Spalding, H. Druid, P. Arner, A. M. J. Shapiro, M. Grompe, A. Aravanis, O. Venn, A. Jamshidi, R. Shemer, Y. Dor, B. Glaser, T. Kaplan, A DNA methylation atlas of normal human cell types. *Nature*, 1–10 (2023).
41. K. O'Neill, E. Pleasance, J. Fan, V. Akbari, G. Chang, K. Dixon, V. Csizmok, S. MacLennan, V. Porter, A. Galbraith, C. J. Grisdale, L. Culibrk, J. H. Dupuis, R. Corbett, J. Hopkins, R. Bowlby, P. Pandoh, D. E. Smailus, D. Cheng, T. Wong, C. Frey, Y. Shen, E. Lewis, L. F. Paulin, F. J. Sedlazeck, J. M. T. Nelson, E. Chuah, K. L. Mungall, R. A. Moore, R. Coope, A. J. Mungall, M. K. McConechy, L. M. Williamson, K. A. Schrader, S. Yip, M. A. Marra, J. Laskin, S. J. M. Jones, Long-read sequencing of an advanced cancer cohort resolves rearrangements, unravels haplotypes, and reveals methylation landscapes. *Cell Genom.* **4**, 100674 (2024).
42. Z. Zhang, Y. Hong, S. Zhang, X. Zhu, L. Liu, X. Liao, H. Gu, H. Fang, J. Shi, Toward the DNA methylation haplotype map of 11 common solid cancers. *Cell Rep.* **44**, 116197 (2025).
43. A. L. Costa, D. Doncevic, Y. Wu, L. Yang, K. H. Man, A.-S. Spreng, H. Winter, M. N. C. Fletcher, B. Radlwimmer, C. Herrmann, A new IDH-independent hypermethylation phenotype is associated with astrocyte-like cell state in glioblastoma. *Genome Biol.* **26**, 192 (2025).
44. Y. Wu, M. Fletcher, Z. Gu, Q. Wang, B. Costa, A. Bertoni, K.-H. Man, M. Schlotter, J. Felsberg, J. Mangei, M. Barbus, A.-C. Gaupel, W. Wang, T. Weiss, R. Eils, M. Weller, H. Liu, G. Reifenberger, A. Korshunov, P. Angel, P. Lichter, C. Herrmann, B. Radlwimmer, Glioblastoma epigenome profiling identifies SOX10 as a master regulator of molecular tumour subtype. *Nat. Commun.* **11**, 6434 (2020).
1. 45. A. Kundaje, W. Meuleman, J. Ernst, M. Bilenky, A. Yen, A. Heravi-Moussavi, P. Kheradpour, Z. Zhang, J. Wang, M. J. Ziller, V. Amin, J. W. Whitaker, M. D. Schultz, L. D. Ward, A. Sarkar, G. Quon, R. S. Sandstrom, M. L. Eaton, Y.-C. Wu, A. Pfenning, X. Wang, M. C. Liu, C. Coarfa, R. A. Harris, N. Shoresh, C. B. Epstein, E. Gjoneska, D. Leung, W. Xie, R. D. Hawkins, R. Lister, C. Hong, P. Gascard, A. J. Mungall, R. Moore, E. Chuah, A. Tam, T. K. Canfield, R. S. Hansen, R. Kaul, P. J. Sabo, M. S. Bansal, A. Carles, J. R. Dixon, K.-H. Farh, S. Feizi, R. Karlic, A.-R. Kim, A. Kulkarni, D. Li, R. Lowdon, G. Elliott, T. R. Mercer, S. J. Neph, V. Onuchic, P. Polak, N. Rajagopal, P. Ray, R. C. Sallari, K. T. Siebenthall, N. A. Sinnott-Armstrong, M. Stevens, R. E. Thurman, J. Wu, B. Zhang, X. Zhou, N. Abdennur, M. Adli, M. Akerman, L. Barrera, J. Antosiewicz-Bourget, T. Ballinger, M. J. Barnes, D. Bates, R. J. A. Bell, D. A. Bennett, K. Bianco, C. Bock, P. Boyle, J. Brinchmann, P. Caballero-Campo, R. Camahort, M. J. Carrasco-Alfonso, T. Charnecki, H. Chen, Z. Chen, J. B. Cheng, S. Cho, A. Chu, W.-Y. Chung, C. Cowan, Q. A. Deng, V. Deshpande, M. Diegel, B. Ding, T. Durham, L. Echipare, L. Edsall, D. Flowers, O. Genbacev-Krtolica, C. Gifford, S. Gillespie, E. Giste, I. A. Glass, A. Gnirke, M. Gormley, H. Gu, J. Gu, D. A. Hafler, M. J. Hangauer, M. Hariharan, M. Hatan, E. Haugen, Y. He, S. Heimfeld, S. Herlofsen, Z. Hou, R. Humbert, R. Issner, A. R. Jackson, H. Jia, P. Jiang, A. K. Johnson, T. Kadlecek, B. Kamoh, M. Kapidzic, J. Kent, A. Kim, M. Kleinewietfeld, S. Klugman, J. Krishnan, S. Kuan, T. Kutyavin, A.-Y. Lee, K. Lee, J. Li,

N. Li, Y. Li, K. L. Ligon, S. Lin, Y. Lin, J. Liu, Y. Liu, C. J. Luckey, Y. P. Ma, C. Maire, A. Marson, J. S. Mattick, M. Mayo, M. McMaster, H. Metsky, T. Mikkelsen, D. Miller, M. Miri, E. Mukame, R. P. Nagarajan, F. Neri, J. Nery, T. Nguyen, H. O'Geen, S. Paithankar, T. Papayannopoulou, M. Pelizzola, P. Plettner, N. E. Propson, S. Raghuraman, B. J. Raney, A. Raubitschek, A. P. Reynolds, H. Richards, K. Riehle, P. Rinaudo, J. F. Robinson, N. B. Rockweiler, E. Rosen, E. Rynes, J. Schein, R. Sears, T. Sejnowski, A. Shafer, L. Shen, R. Shoemaker, M. Sigaroudinia, I. Slukvin, S. Stehling-Sun, R. Stewart, S. L. Subramanian, K. Suknuntha, S. Swanson, S. Tian, H. Tilden, L. Tsai, M. Urich, I. Vaughn, J. Vierstra, S. Vong, U. Wagner, H. Wang, T. Wang, Y. Wang, A. Weiss, H. Whitton, A. Wildberg, H. Witt, K.-J. Won, M. Xie, X. Xing, I. Xu, Z. Xuan, Z. Ye, C. Yen, P. Yu, X. Zhang, X. Zhang, J. Zhao, Y. Zhou, J. Zhu, Y. Zhu, S. Ziegler, A. E. Beaudet, L. A. Boyer, P. L. D. Jager, P. J. Farnham, S. J. Fisher, D. Haussler, S. J. M. Jones, W. Li, M. A. Marra, M. T. McManus, S. Sunyaev, J. A. Thomson, T. D. Tlsty, L.-H. Tsai, W. Wang, R. A. Waterland, M. Q. Zhang, L. H. Chadwick, B. E. Bernstein, J. F. Costello, J. R. Ecker, M. Hirst, A. Meissner, A. Milosavljevic, B. Ren, J. A. Stamatoyannopoulos, T. Wang, M. Kellis, A. Kundaje, W. Meuleman, J. Ernst, M. Bilenky, A. Yen, A. Heravi-Moussavi, P. Kheradpour, Z. Zhang, J. Wang, M. J. Ziller, V. Amin, J. W. Whitaker, M. D. Schultz, L. D. Ward, A. Sarkar, G. Quon, R. S. Sandstrom, M. L. Eaton, Y.-C. Wu, A. R. Pfenning, X. Wang, M. Claussnitzer, Y. Liu, C. Coarfa, R. A. Harris, N. Shoresh, C. B. Epstein, E. Gjoneska, D. Leung, W. Xie, R. D. Hawkins, R. Lister, C. Hong, P. Gascard, A. J. Mungall, R. Moore, E. Chuah, A. Tam, T. K. Canfield, R. S. Hansen, R. Kaul, P. J. Sabo, M. S. Bansal, A. Carles, J. R. Dixon, K.-H. Farh, S. Feizi, R. Karlic, A.-R. Kim, A. Kulkarni, D. Li, R. Lowdon, G. Elliott, T. R. Mercer, S. J. Neph, V. Onuchic, P. Polak, N. Rajagopal, P. Ray, R. C. Sallari, K. T. Siebenthall, N. A. Sinnott-Armstrong, M. Stevens, R. E. Thurman, J. Wu, B. Zhang, X. Zhou, A. E. Beaudet, L. A. Boyer, P. L. D. Jager, P. J. Farnham, S. J. Fisher, D. Haussler, S. J. M. Jones, W. Li, M. A. Marra, M. T. McManus, S. Sunyaev, J. A. Thomson, T. D. Tlsty, L.-H. Tsai, W. Wang, R. A. Waterland, M. Q. Zhang, L. H. Chadwick, B. E. Bernstein, J. F. Costello, J. R. Ecker, M. Hirst, A. Meissner, A. Milosavljevic, B. Ren, J. A. Stamatoyannopoulos, T. Wang, M. Kellis, Integrative analysis of 111 reference human epigenomes. *Nature* **518**, 317–330 (2015).

45. M. Chen, R. Fu, Y. Chen, L. Li, S.-W. Wang, High-resolution, noninvasive single-cell lineage tracing in mice and humans based on DNA methylation epimutations. *Nat. Methods*, 1–11 (2025).

46. M. Scherer, I. Singh, M. M. Braun, C. Szu-Tu, P. S. Sanchez, D. Lindenhofer, N. A. Jakobsen, V. Körber, M. Kardorff, L. Nitsch, P. Kautz, J. Rühle, A. Bianchi, L. Cozzuto, R. Frömel, S. Beneyto-Calabuig, C. Lareau, A. T. Satpathy, R. Beekman, L. M. Steinmetz, S. Raffel, L. S. Ludwig, P. Vyas, A. Rodriguez-Fraticelli, L. Velten, Clonal tracing with somatic epimutations reveals dynamics of blood ageing. *Nature* **643**, 478–487 (2025).

Acknowledgements:

We thank the Miga laboratory at University of California-Santa Cruz for assistance generating the ONT data, M. Jain at Northeastern University for consulting on ONT data analysis, and A. Stergachis at the University of Washington for reagents and assistance with Fiber-seq.

1058 Hematopoietic stem cells were purchased from the Cooperative Centers of Excellence in
1059 Hematology at the Fred Hutchinson Cancer Center, which is supported in part by NIDDK Grant #
1060 DK106829. We are grateful to the patients and research subjects at Alvin J. Siteman Cancer Center
1061 at Washington University School of Medicine and Barnes-Jewish Hospital in St. Louis for their
1062 participation in the Genomics of AML banking study, which is supported by WashU AML SPORE
1063 (P50CA171963, Daniel C. Link, PI), and thank the Siteman Cancer Center for the use of the
1064 Siteman Tissue Procurement and Flow Cytometry Cores. The Siteman Cancer Center is supported
1065 in part by an NCI Cancer Center Support Grant P30CA091842. We also thank D. Russler-Germain,
1066 A. Young, and J. Edwards at Wash U for helpful comments when preparing this manuscript.

1067 **Funding:**

1068 This work was supported by National Institutes of Health grants R00GM140251 to MPM and
1069 R37CA259359 to DHS.

1070 **Author contributions:**

1071 Conceptualization: MM, DHS
1072 Resources: DHS
1073 Investigation: MM, HJA, ND, HS, EK, BJ, CM, CF, RF, MPM, DHS
1074 Funding acquisition: DHS
1075 Project administration: DHS
1076 Visualization: MM, HJA, DHS
1077 Writing – original draft: MM, DHS
1078 Writing – review & editing: All authors

1079 **Competing interests:**

1080 None

1081 **Data and materials availability:**

1082 Raw and processed genomic data has been deposited to dbGaP (PHS000159) and GEO (accession

1083 pending), respectively.

1084